GENERAL DISTRIBUTION
OCDE/GD(94)21
NEA/NSC/DOC(93)5

SENSITIVITIES OF CALCULATED CROSS SECTIONS OF ^{56}Fe TO MODEL PARAMETERS

by
K. Shibata

ORGANISATION FOR ECONOMIC CO-OPERATION AND DEVELOPMENT
Paris 1994

GENERAL DISTRIBUTION

OCDE/GD(94)21

NEA/NSC/DOC(93)5

SENSITIVITIES OF CALCULATED CROSS SECTIONS OF Fe56 to MODEL PARAMETERS

K.SHIBATA

OECD Nuclear Energy Agency

France

ORGANISATION FOR ECONOMIC CO-OPERATION AND DEVELOPMENT

Paris 1994

012428

NUCLEAR SCIENCE

DOC(1993)5

Sensitivities of Calculated Cross Sections of ^{56}Fe to Model Parameters

K. Shibata
OECD/NEA Data Bank
Issy-les-Moulineaux, FRANCE

Abstract

Sensitivities of nuclear model calculations to input parameters are obtained using optical and statistical model codes. There is no code dependence on the sensitivities of the optical model calculations. The calculated $^{56}Fe(n,px)$ and $^{56}Fe(n,\alpha x)$ reaction cross sections are found to be very sensitive to the level density parameters for the target nucleus. Model parameter sensitivities are one type of additional information that may be stored in future cross-section evaluations together with parameter uncertainties.

1. Introduction

Nuclear-model calculations have been widely used to create evaluated neutron cross-section libraries. In particular, multi-step Hauser-Feshbach codes enable one to calculate all the necessary cross sections up to an incident energy of 20 MeV. Existing neutron cross-section libraries are to a large extent based on these calculations. There are however a lot of parameters required as input to the codes, such as optical-model parameters, level density parameters, giant-dipole resonance parameters for gamma-ray emission and the parameter for the residual interaction in the preequilibrium mode. Although each evaluator makes much effort to determine the values for these parameters, it is not so clear how much they affect the calculated results. If one tries to calculate sensitivities of the results to input-parameters, it will be necessary to make a lot of calculation by varying each parameter, which is tedious and time-consuming.

A precompiler named GRESS [1] was developed at ORNL to enhance FORTRAN programs by adding the calculation of derivatives along with the original output. In the present work, the code TNG [2], which is one of the multi-step Hauser-Feshbach codes developed at ORNL, was modified using the precompiler GRESS and was used to calculate the sensitivities of the neutron-induced reaction cross sections of ^{56}Fe to input parameters.

Section 2 describes the parameters used in the sensitivity calculation. The calculated results are presented in Section 3.

2. Computational Methods and Procedures

In the present work, we used a multi-step Hauser-Feshbach code TNG to calculate the cross sections of ^{56}Fe. The calculated reactions are given as follows:

	1st step	2nd step
n + ^{56}Fe	→ n + ^{56}Fe	→ n + γ + ^{56}Fe
		→ 2n + ^{55}Fe
		→ n + p + ^{55}Mn
		→ n + α + ^{52}Cr
	→ p + ^{56}Mn	→ p + γ + ^{56}Mn
		→ p + n + ^{55}Mn
	→ α + ^{53}Cr	→ α + γ + ^{53}Cr
		→ α + n + ^{52}Cr.

The input data to the code were taken from the evaluation work of ^{56}Fe [3] for ENDF/B-V, and they are given in Tables 1-3. Cascade γ-emission was calculated for each residual nucleus. The parameter for the residual two-body interaction in the precompound process, which is referred to as precompound parameter hereafter, was set to be 400 MeV^3. The direct interaction for the inelastic scattering was neglected in the present analyses. Figures 1-3 show the calculated (n,nx), (n,px) and (n,αx) reaction cross sections, respectively.

Calculated were the sensitivities of the cross sections to optical-model, level-density, giant-dipole resonance and precompound parameters. One of the optical-model codes, SCAT-2 [4], was employed to examine the code dependence on the sensitivities to the optical-model parameters.

The GRESS code modified the codes TNG and SCAT-2 by adding the routines of the calculation of derivatives with respect to input data. The GRESS code yields the normalized sensitivities which are obtained by multiplying a derivative by its associated input parameter value and dividing by the associated output value. A normalized sensitivity of 0.1 means that a 1% change in that input parameter would induce a 0.1% change in the output. The GRESS code accepts a majority of ANSI X3.9-1978 standard FORTRAN-77. However, there are several limitations for its application. One big limitation is that GRESS is unable to deal with complex functions. Optical-model codes usually have complex functions within them. In the present case, all the complex functions and variables in the optical-model part of TNG were converted to real functions and variables. According to the author's experience, the modified code sometimes produced overflow errors which had to be fixed.

3. Calculated Sensitivities

3.1 Optical-model parameters

The sensitivities of the total, shape elastic scattering and compound nucleus formation cross sections were calculated with respect to neutron optical-model parameters, i.e., depths, radii and diffuseness for real and imaginary potentials in the incident energy range from 100 keV to 20 MeV. The calculated results obtained with TNG are shown in Figs. 4-9. It is found from the figures that the sensitivities to the diffuseness parameters are smaller than those to other parameters. Figures 10-15 show

the calculations obtained with SCAT-2. It should be noted that the two sets of the results obtained from the two independent codes are almost consistent with each other, which means that there is no code dependence on the sensitivities if the same physical model is employed.

The sensitivities of the first step Hauser-Feshbach calculations are shown in Figs. 16-18. Real radius parameters affect the calculated cross sections considerably.

3.2 Level-density parameters

The effects of the level-density parameters were calculated on the neutron-, proton- and alpha-emission cross sections (first step in the multi-step reactions). Considered were the $\underline{a}$ parameters, spin cut-off factors and pairing corrections for the nuclei ^{56}Fe, ^{56}Mn and ^{53}Cr. As for the neutron emission, its cross section is sensitive to the $\underline{a}$ parameters for ^{56}Fe and ^{56}Mn, as seen in Fig. 19. Figures 20 and 21 indicate that the proton and alpha emission cross sections are sensitive not only to the $\underline{a}$ parameters for their residual nuclei ^{56}Mn and ^{53}Cr but also to that for the target nucleus ^{56}Fe.

3.3 Precompound parameter

Figure 22 shows that the cross sections are not sensitive to the precompound parameter. However, it is found from Fig. 23 that the higher energy part of neutron spectrum is much influenced by the parameter. This phenomenon is understandable by the preequilibrium theory.

3.4 Giant-dipole resonance parameters

Figures 24-26 show the sensitivities of (n,nx), (n,px) and (n,αx) cross sections with respect to giant-dipole resonance parameters. Comparing these figures with Figs. 1-3, it is found that the sensitivity is large near the threshold and becoming smaller with incident energy.

4. Uncertainty of Cross Sections

The sensitivity of the cross sections is large with respect to the real radius parameter of the optical model potential and to the level density parameter $\underline{a}$ for the target nucleus. If one knows the uncertainty of these parameters, it is possible to obtain the uncertainty of the calculated cross sections.

Figures 27-29 show the calculated emission spectra together with their uncertainties. In these figures, ±1% was assumed for an error of each radius parameter. The proton and α emission cross sections are found to have large uncertainties compared with neutron emission cross sections.

Figures 30-41 show the variance of the calculated cross sections by assuming ±1% error for the a parameter for ^{56}Fe. Large spread is seen in the (n,p) and (n,α) channels.

5. Conclusions

The sensitivities of nuclear-model calculations to input parameters were obtained by using the TNG and SCAT-2 codes. The precompiler GRESS modified the FORTRAN-77 source programs of TNG and SCAT-2 by adding functions of calculating derivatives.

Concerning the total, compound-nucleus formation and shape elastic scattering cross sections calculated with the optical model, the two independent codes yielded the same sensitivities although coding of the programs is completely different. This fact indicated that there is no code dependence on the sensitivities as far as the same physical model is involved.

The level density parameters affects the Hauser-Feshbach calculations considerably. Among the parameters, the a parameter for the target nucleus produces the largest effect on all the cross sections in the energy range from 6 to 20 MeV.

Acknowledgment

The author would like to thank Dr. E. Sartori of the NEA Data Bank for his encouragement during this work.

References

1. J.E. Horwedel: "GRESS Version 2.0 User's Manual", ORNL/TM-1191 (1991).

2. K. Shibata and C.Y. Fu: "Recent Improvements of the TNG Statistical Model Code", ORNL/TM-10093 (1986); C.Y. Fu: "A Consistent Nuclear Model for Compound and Precompound Reactions with Conservation of Angular Momentum", ORNL/TM-7042 (1980).

3. C.Y. Fu and D.M. Hetrick: "Update of ENDF/B-V Mod-3 Iron: Neutron-Producing Reaction Cross Sections and Energy-Angle Correlations", ORNL/TM-9964 (1986).

4. O. Bersillon: "The Computer Code SCAT-2", Proc. Workshop on Applied Nuclear Theory and Nuclear Model Calculations for Nuclear Technology Applications, p. 319, World Scientific (1989).

5. F.D. Becchetti, Jr. and G.W. Greenlees: Phys. Rev. 182, 1190 (1969).

6. J.R. Huizenga and G. Igo: Nucl. Phys., 29, 462 (1962).

Table 1 Optical-model potential parameters

Neutrons [3]

$V = 49.747 - 0.4295 \times E - 0.0003 \times E^2$ (MeV)
$W_s = 11.8 - 0.21 \times E$ (MeV)
$r_0 = 1.287$ (fm), $r_s = 1.345$ (fm)
$a_0 = 0.56$ (fm), $a_s = 0.47$ (fm)

Protons [5]

$V = 54.0 + 0.4 \times Z / A^{1/3} + 24.0 \times \eta - 0.32 \times E$ (MeV)
$W_s = 11.8 + 12.0 \times \eta - 0.25 \times E$ (MeV)
$W_v = 0.22 \times E - 2.7$ (MeV)
$r_0 = 1.17$ (fm), $r_s = 1.32$ (fm)
$r_v = 1.32$ (fm), $r_c = 1.25$ (fm)
$a_0 = 0.75$ (fm), $a_s = 0.51 + 0.7 \times \eta$ (fm)
$a_v = a_s$

α-particles [6]

$V = 50.0$ (MeV), $W_v = 5.7 + 0.087 \times A$ (MeV)
$r_0 = 1.17 + 1.77 / A^{1/3}$ (fm), $r_v = r_0$
$r_c = 1.17$ (fm)
$a_0 = 0.576$ (fm), $a_v = 0.576$ (fm)

Z = atomic number, A = mass number , N = A - Z and $\eta = (N - Z)/A$

Table 2 Level density parameters

Residual nuclei	T (MeV)	E_0 (MeV)	a (1/MeV)	Δ (MeV)	c	E_c (MeV)	E_x (MeV)
^{56}Fe	1.417	-0.105	6.355	2.810	8.260	4.539	10.750
^{55}Fe	1.509	-1.483	5.909	1.540	7.589	3.076	9.859
^{56}Mn	1.256	-2.200	7.233	0.525	9.401	0.754	7.676
^{55}Mn	1.289	-1.045	6.665	1.270	8.560	2.570	7.920
^{53}Cr	1.288	-0.762	6.500	1.350	8.144	2.681	7.673
^{52}Cr	1.392	-0.183	6.154	2.650	7.613	3.700	9.794

T = nuclear temperature
E_0 = parameter for matching lower energy level density to the higher one
Δ = pairing energy correction
E_c = continuum cut-off
E_x = tagency point
$c = 0.0888 \times a \times A^{2/3}$ (spin cut-off factor)

Table 3 Giant dipole resonance

Absorption cross section for giant dipole

$$\sigma^{E1}(E_\gamma) = \sigma_m E_\gamma^2 \Gamma^2 / [(E_\gamma^2 - E_m^2)^2 + E_\gamma^2 \Gamma^2]$$

Parameters in the cross section

$\sigma_m = 168NZ/(\pi\Gamma A)$ (mb)
$E_m = 163(NZ)^{1/2}/A^{4/3}$ (MeV)
$\Gamma = 5.0$ (MeV)

Z = atomic number, A = mass number and N = A - Z

Figure Captions

Fig. 1 $^{56}Fe(n,nx)$ reaction cross sections calculated with TNG

Fig. 2 $^{56}Fe(n,px)$ reaction cross sections calculated with TNG

Fig. 3 $^{56}Fe(n,\alpha x)$ reaction cross sections calculated with TNG

Fig. 4 Sensitivity of optical-model calculations to real well depth obtained by TNG

Fig. 5 Sensitivity of optical-model calculations to imaginary well depth obtained by TNG

Fig. 6 Sensitivity of optical-model calculations to real radius obtained by TNG

Fig. 7 Sensitivity of optical-model calculations to imaginary radius obtained by TNG

Fig. 8 Sensitivity of optical-model calculations to real diffuseness obtained by TNG

Fig. 9 Sensitivity of optical-model calculations to imaginary diffuseness obtained by TNG

Fig. 10 Sensitivity of optical-model calculations to real well depth obtained by SCAT-2

Fig. 11 Sensitivity of optical-model calculations to imaginary well depth obtained by SCAT-2

Fig. 12 Sensitivity of optical-model calculations to real radius obtained by SCAT-2

Fig. 13 Sensitivity of optical-model calculations to imaginary radius obtained by SCAT-2

Fig. 14 Sensitivity of optical-model calculations to real diffuseness obtained by SCAT-2

Fig. 15 Sensitivity of optical-model calculations to imaginary diffuseness obtained by SCAT-2

Fig. 16 Sensitivity of $^{56}Fe(n,n')$ reaction cross sections to optical model parameters
The symbols VN, RVN, AVN, WN, RWN and AWN stand for real depth, real radius, real diffuseness, imaginary depth, imaginary radius and imaginary diffuseness for neutron potentials, respectively.

Fig. 17 Sensitivity of $^{56}Fe(n,p)$ reaction cross sections to optical model parameters
The symbols VP, RVP, AVP, WP, RWP and AWP stand for real depth, real radius, real diffuseness, imaginary depth, imaginary radius and imaginary diffuseness for proton potentials, respectively.
For the remaining symbols, see the caption of Fig. 16.

Fig. 18 Sensitivity of $^{56}Fe(n,\alpha)$ reaction cross sections to optical model parameters
The symbols VA, RVA, AVA, WA, RWA and AWA stand for real depth, real radius, real diffuseness, imaginary depth, imaginary radius and imaginary diffuseness for α-particle potentials, respectively. For the remaining symbols, see the caption of Fig. 16.

Fig. 19 Sensitivity of $^{56}Fe(n,n')$ reaction cross section to level density parameters
The symbols a, c and p stand for a, spin cut-off and pairing energy correction parameters.

Fig. 20 Sensitivity of $^{56}Fe(n,p)$ reaction cross sections to level density parameters
The symbols a, c and p stand for a, spin cut-off and pairing energy correction parameters.

Fig. 21 Sensitivity of $^{56}Fe(n,\alpha)$ reaction cross sections to level density parameters
The symbols a, c and p stand for a, spin cut-off and pairing energy correction parameters.

Fig. 22 Sensitivity of (n,n'), (n,p) and (n,α) reaction cross sections to precompound parameter

Fig. 23 Sensitivity of continuum neutron spectrum at 14.5 MeV to precompound parameter

Fig. 24 Sensitivity of $^{56}Fe(n,nx)$ reaction cross sections to giant dipole resonance parameters

Fig. 25 Sensitivity of $^{56}Fe(n,px)$ reaction cross sections to giant dipole resonance parameters

Fig. 26 Sensitivity of $^{56}Fe(n,\alpha x)$ reaction cross sections to giant dipole resonance parameters

Fig. 27 Neutron emission spectrum at 14.5 MeV
Uncertainty of $\pm 1\%$ was assumed for the real radius of the neutron potentials.

Fig. 28 Proton emission spectrum at 14.5 MeV
Uncertainty of $\pm 1\%$ was assumed for the real radius of the proton potentials.

Fig. 29 α-particle emission spectrum at 14.5 MeV
Uncertainty of $\pm 1\%$ was assumed for the real radius of the α-particle potentials.

Fig. 30 $^{56}Fe(n,n\gamma)$ reaction cross section
Uncertainty of $\pm 1\%$ was assumed for the a parameter for ^{56}Fe.

Fig. 31 $^{56}Fe(n,2n)$ reaction cross section
Uncertainty of $\pm 1\%$ was assumed for the a parameter for ^{56}Fe.

Fig. 32 $^{56}Fe(n,np)$ reaction cross section
Uncertainty of $\pm 1\%$ was assumed for the a parameter for ^{56}Fe.

Fig. 33 $^{56}Fe(n,n\alpha)$ reaction cross section
Uncertainty of ±1% was assumed for the a parameter for ^{56}Fe.

Fig. 34 $^{56}Fe(n,p\gamma)$ reaction cross section
Uncertainty of ±1% was assumed for the a parameter for ^{56}Fe.

Fig. 35 $^{56}Fe(n,pn)$ reaction cross section
Uncertainty of ±1% was assumed for the a parameter for ^{56}Fe.

Fig. 36 $^{56}Fe(n,\alpha\gamma)$ reaction cross section
Uncertainty of ±1% was assumed for the a parameter for ^{56}Fe.

Fig. 37 $^{56}Fe(n,\alpha n)$ reaction cross section
Uncertainty of ±1% was assumed for the a parameter for ^{56}Fe.

Fig. 38 Neutron emission spectrum at 14.5 MeV
Uncertainty of ±1% was assumed for the a parameter for ^{56}Fe.

Fig. 39 Proton emission spectrum at 14.5 MeV
Uncertainty of ±1% was assumed for the a parameter for ^{56}Fe.

Fig. 40 α-particle emission spectrum at 14.5 MeV
Uncertainty of ±1% was assumed for the a parameter for ^{56}Fe.

Fig. 41 γ-ray emission spectrum at 14.5 MeV
Uncertainty of ±1% was assumed for the a parameter for ^{56}Fe.

Fig. 1 ^{56}Fe(n,nx) reaction cross sections calculated with TNG

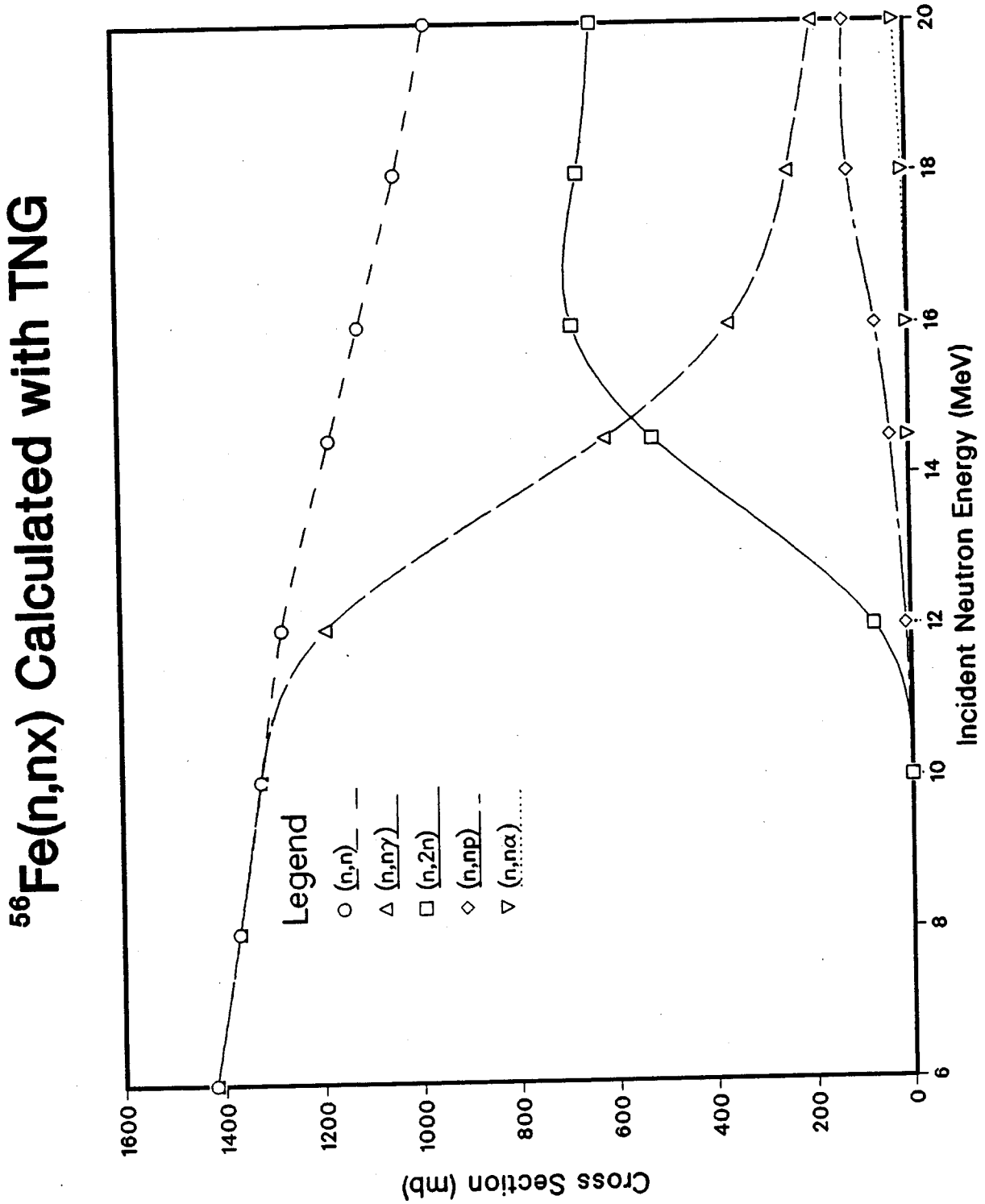

Fig. 2 ^{56}Fe(n,px) reaction cross sections calculated with TNG

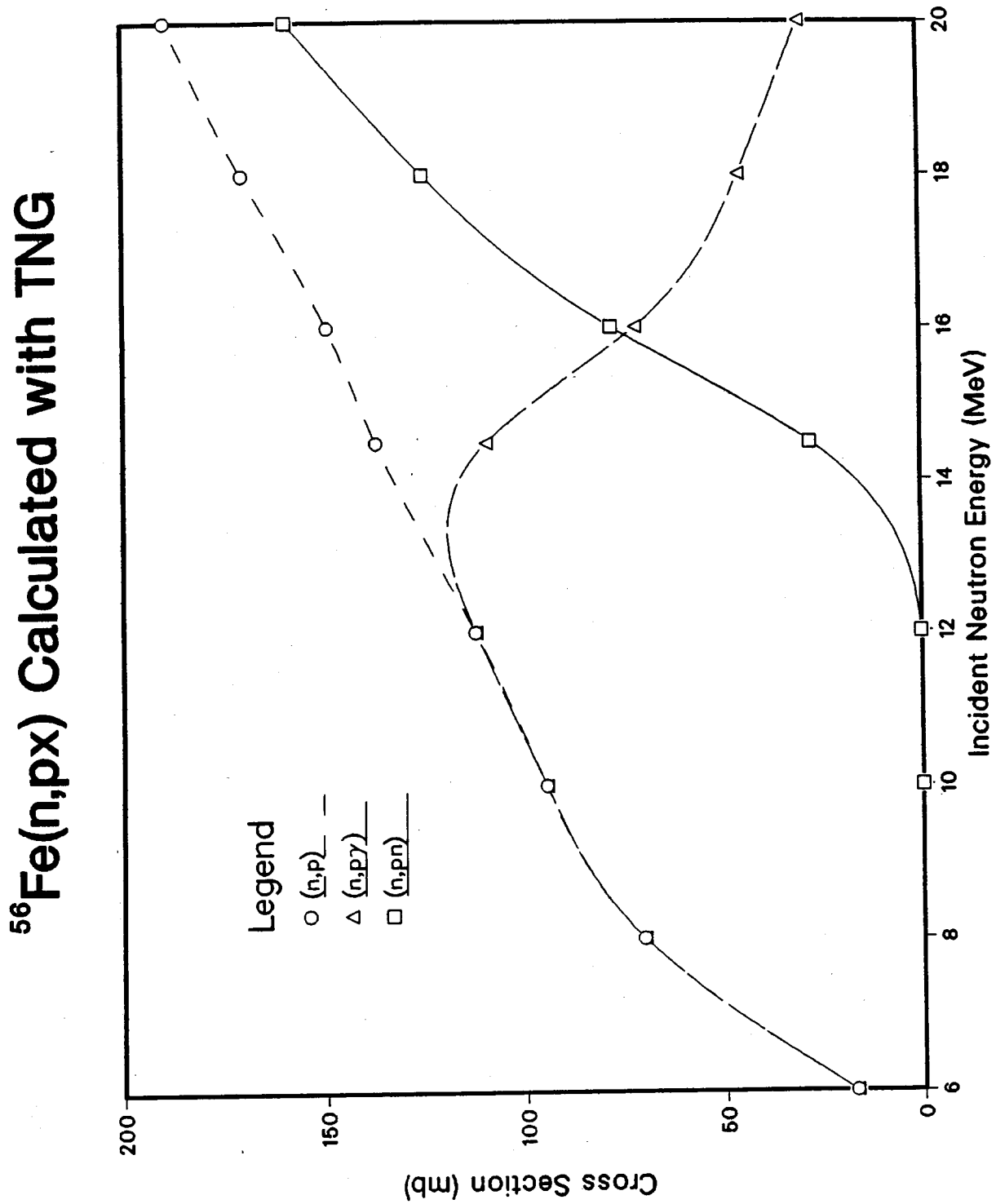

Fig. 3 $^{56}Fe(n,\alpha x)$ reaction cross sections calculated with TNG

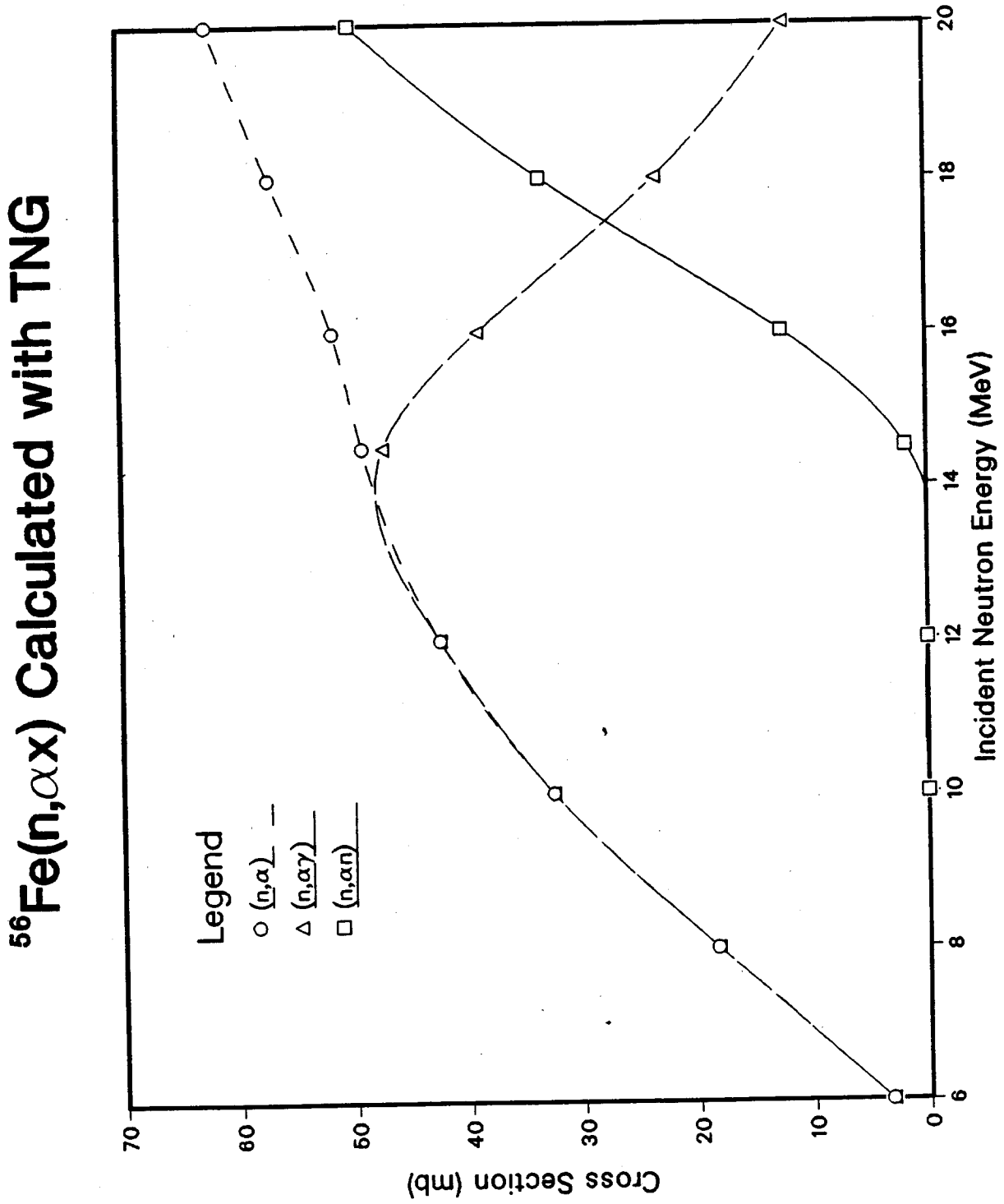

Fig. 4 Sensitivity of optical-model calculations to real well depth obtained by TNG

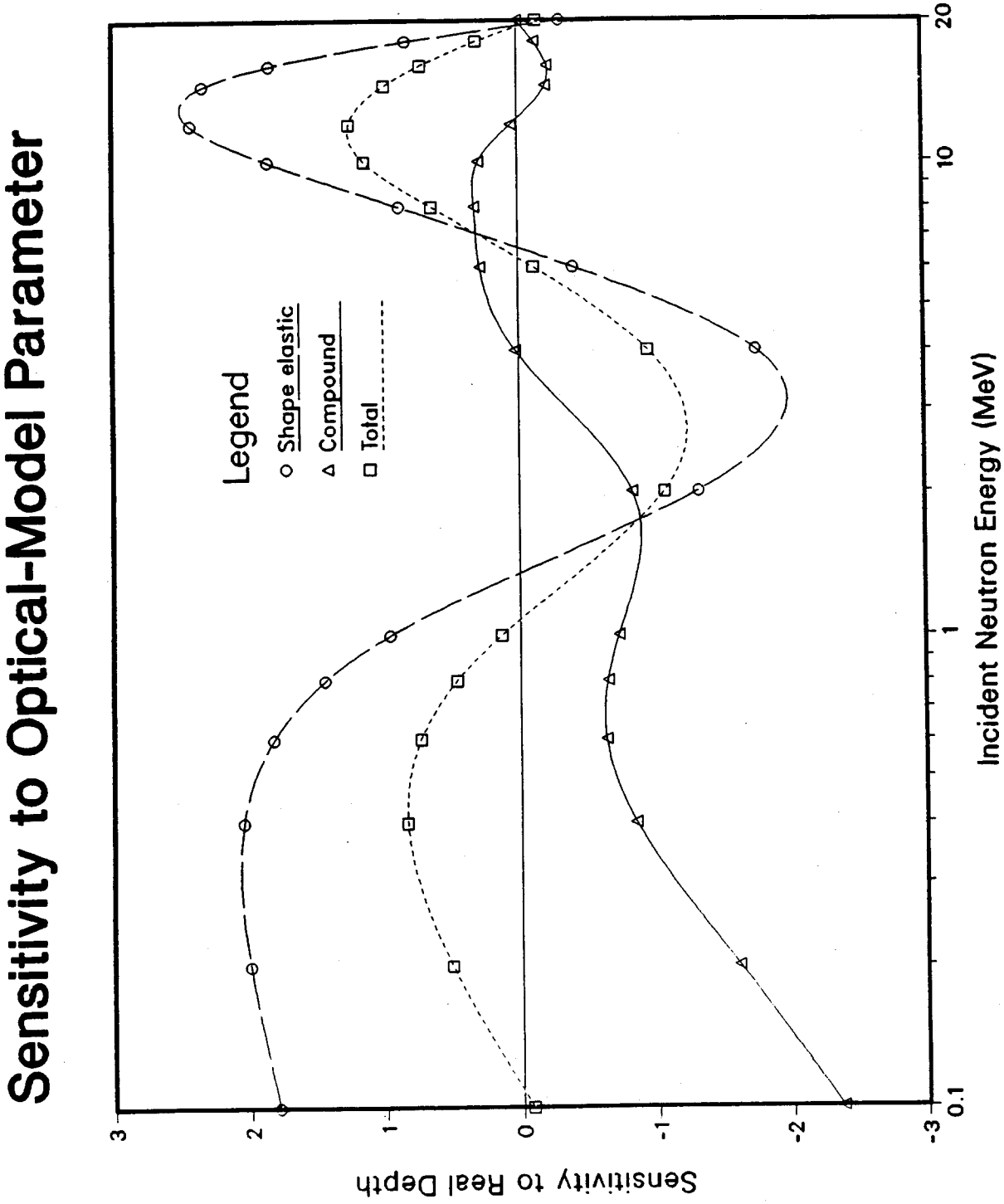

Fig. 5 Sensitivity of optical-model calculations to imaginary well depth obtained by TNG

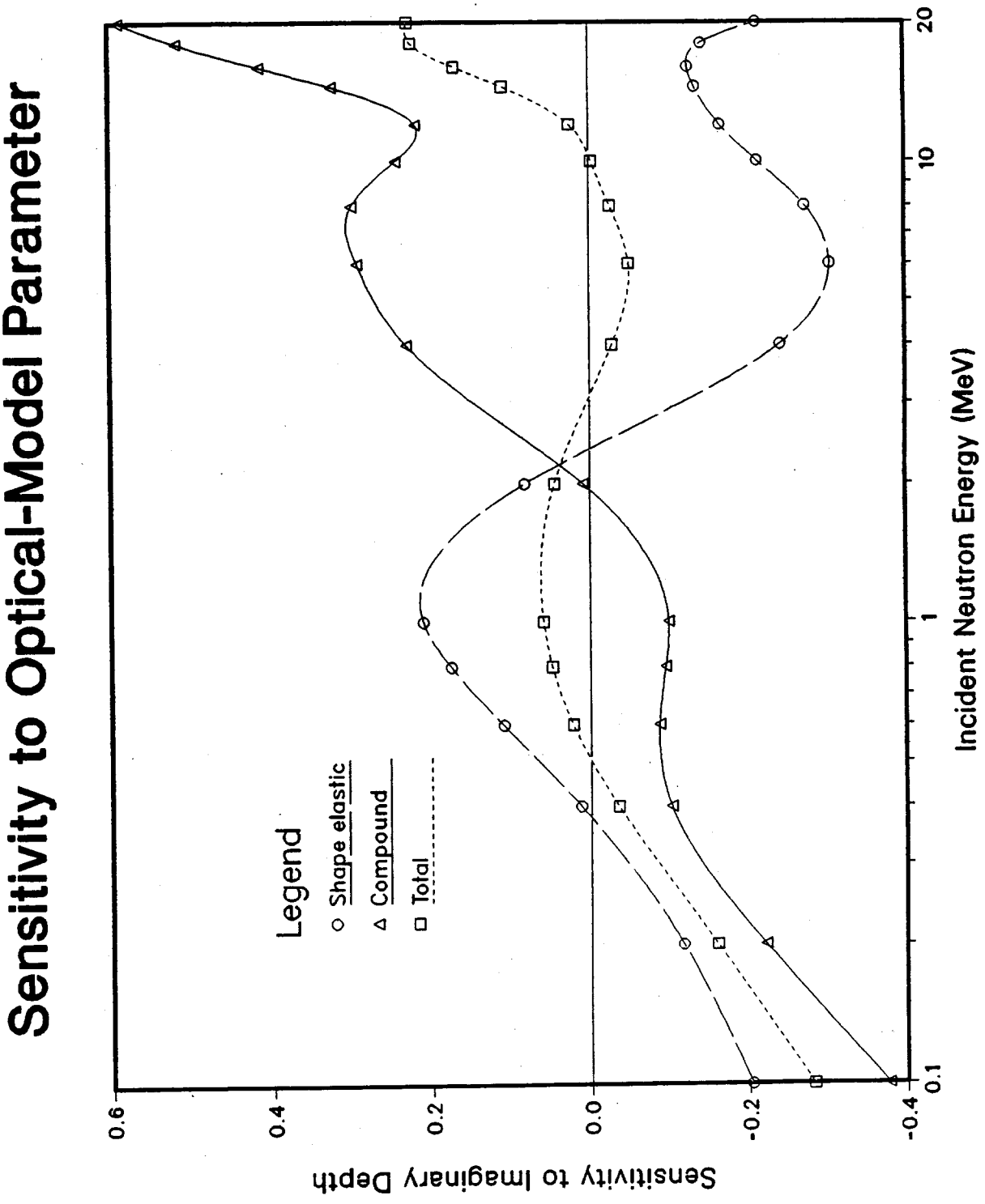

Fig. 6 Sensitivity of optical-model calculations to real radius obtained by TNG

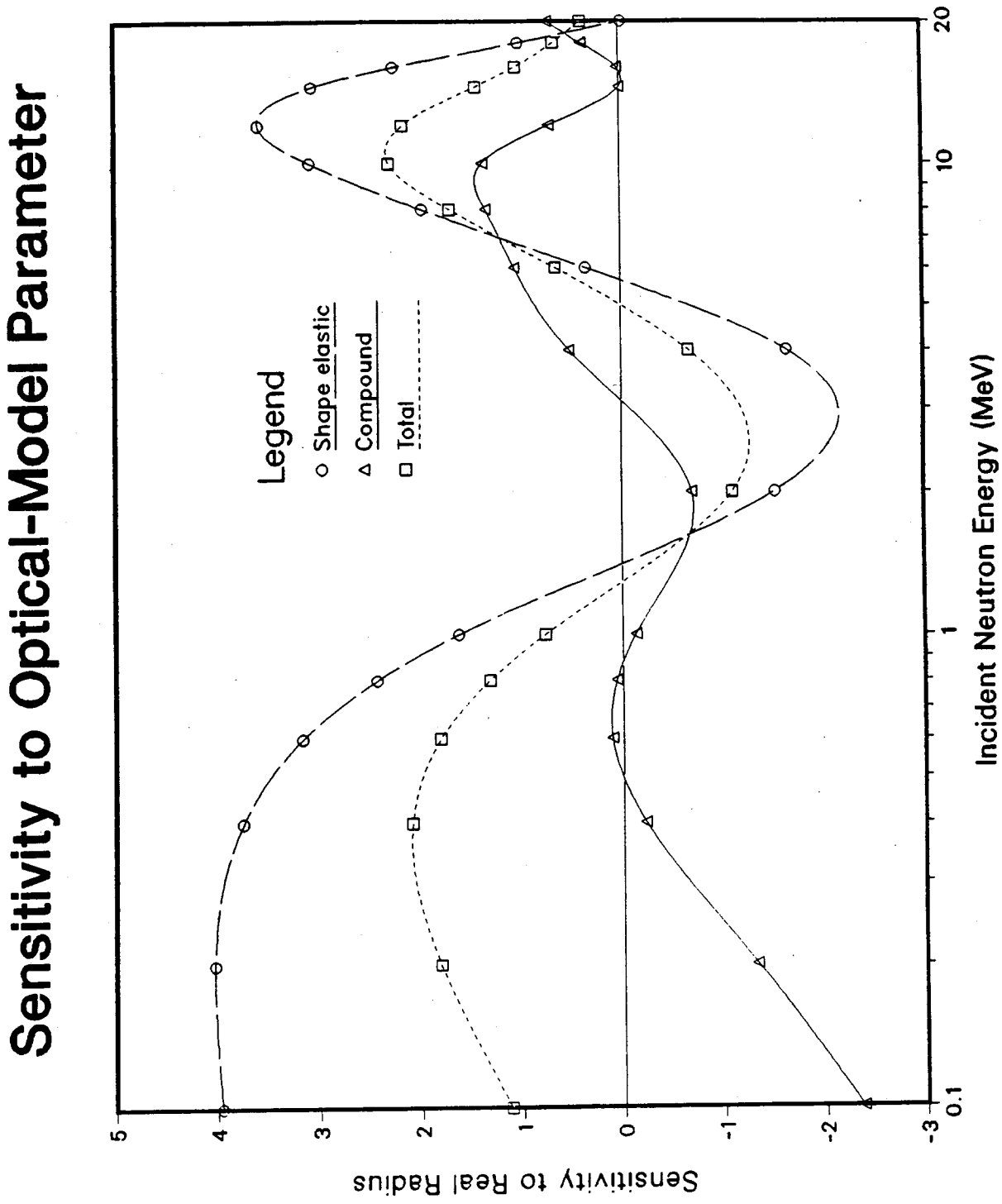

Fig. 7 Sensitivity of optical-model calculations to imaginary radius obtained by TNG

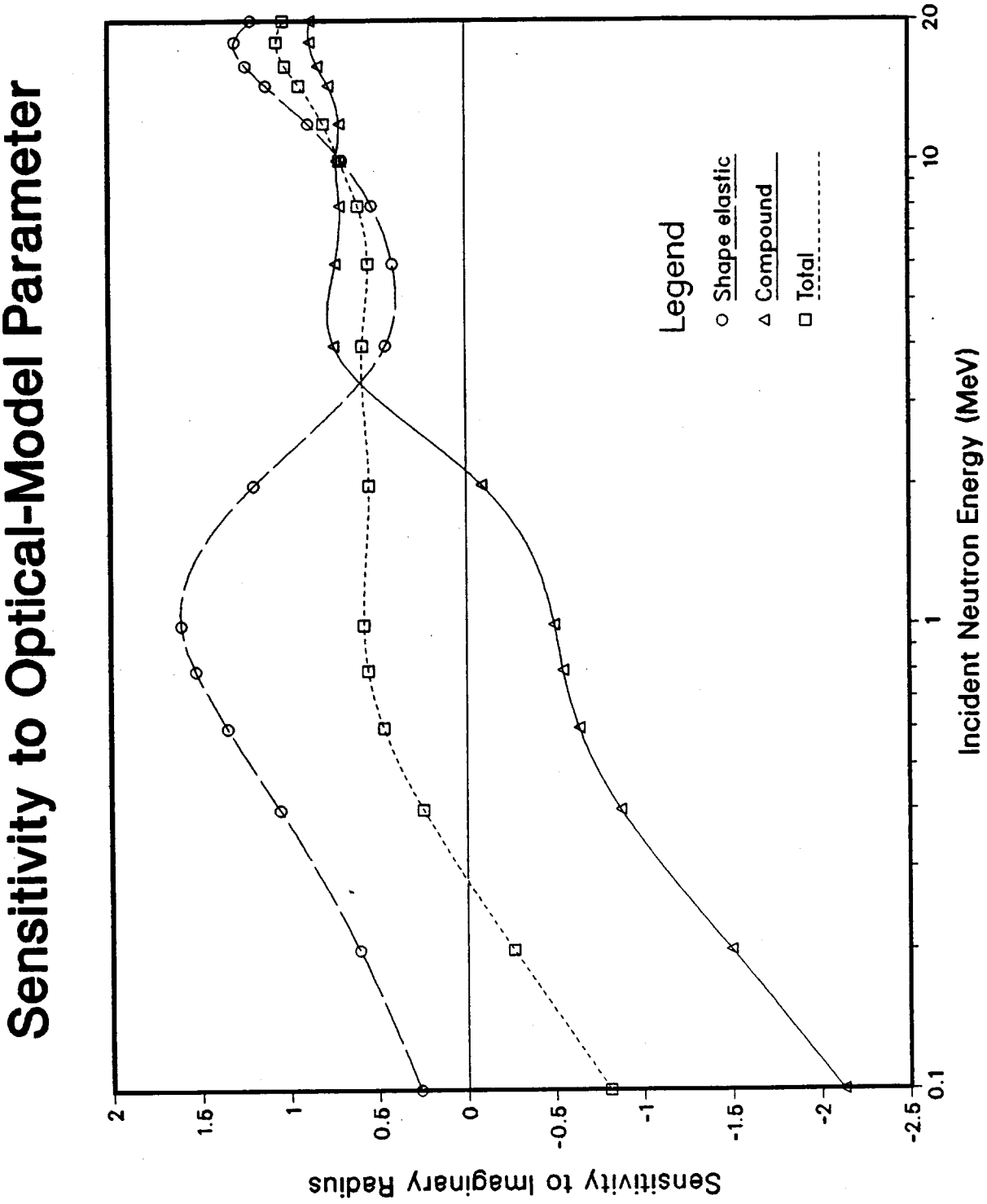

Fig. 8 Sensitivity of optical-model calculations to real diffuseness obtained by TNG

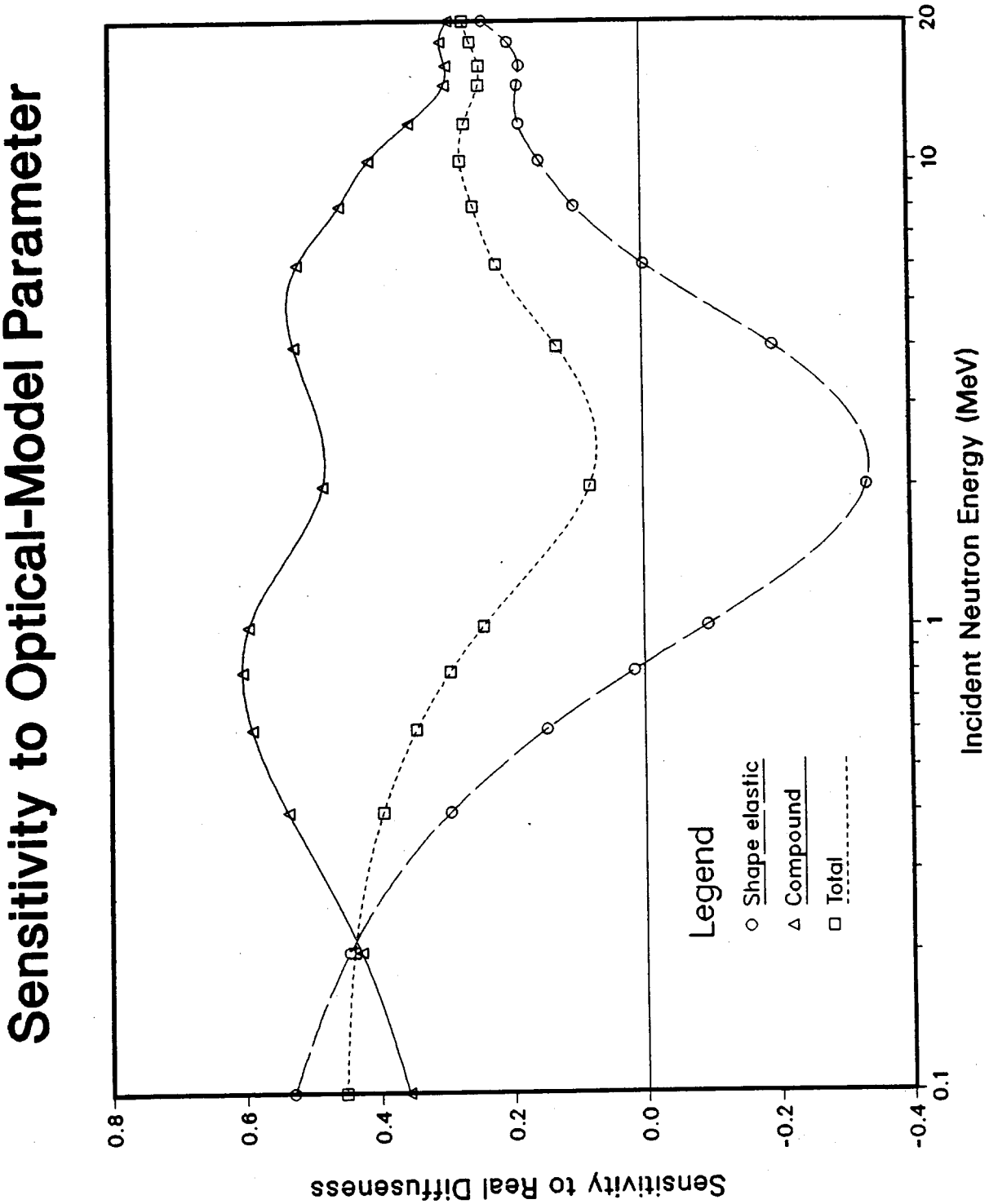

Fig. 9 Sensitivity of optical-model calculations to imaginary diffuseness obtained by TNG

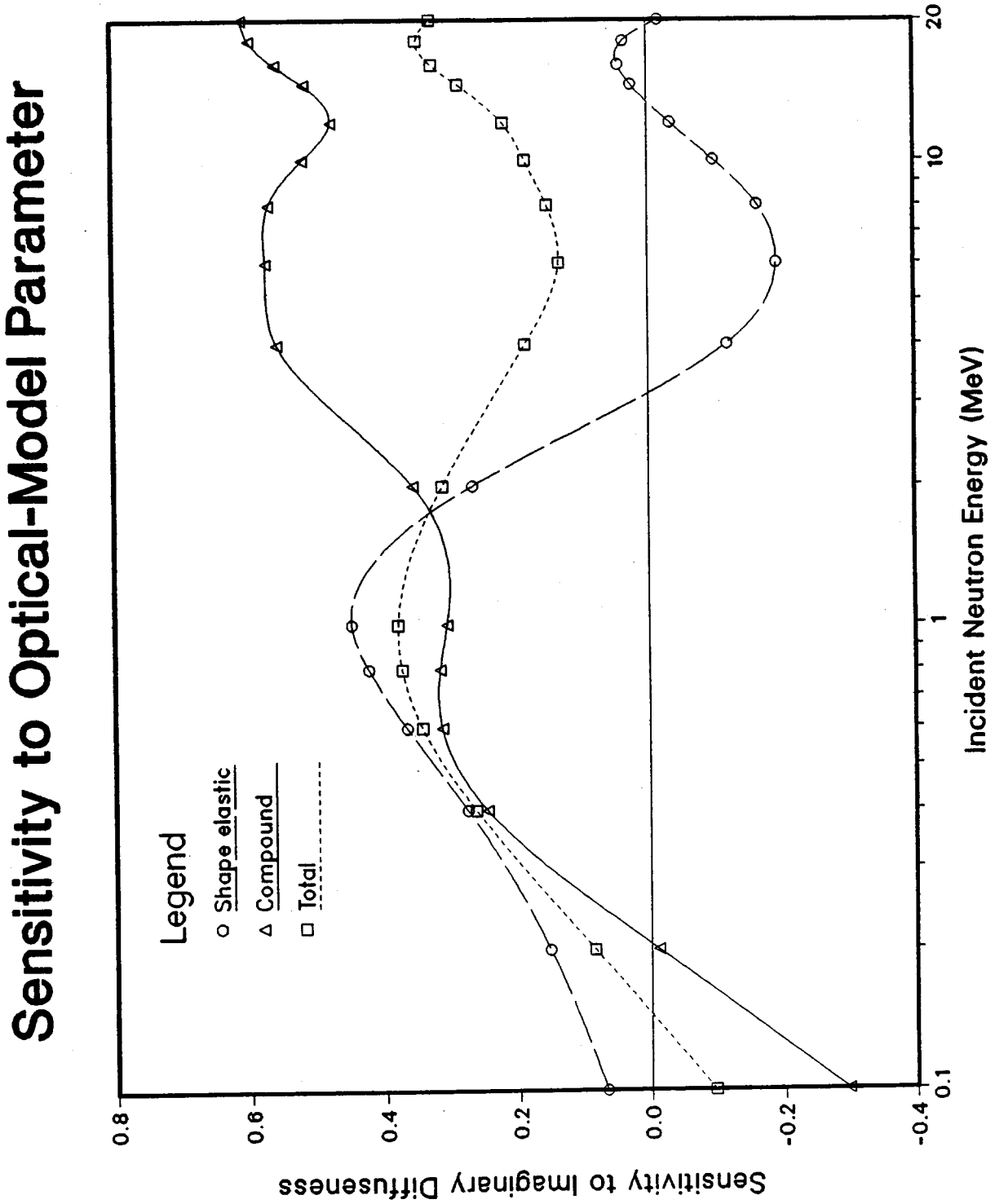

Fig. 10 Sensitivity of optical-model calculations to real well depth obtained by SCAT-2

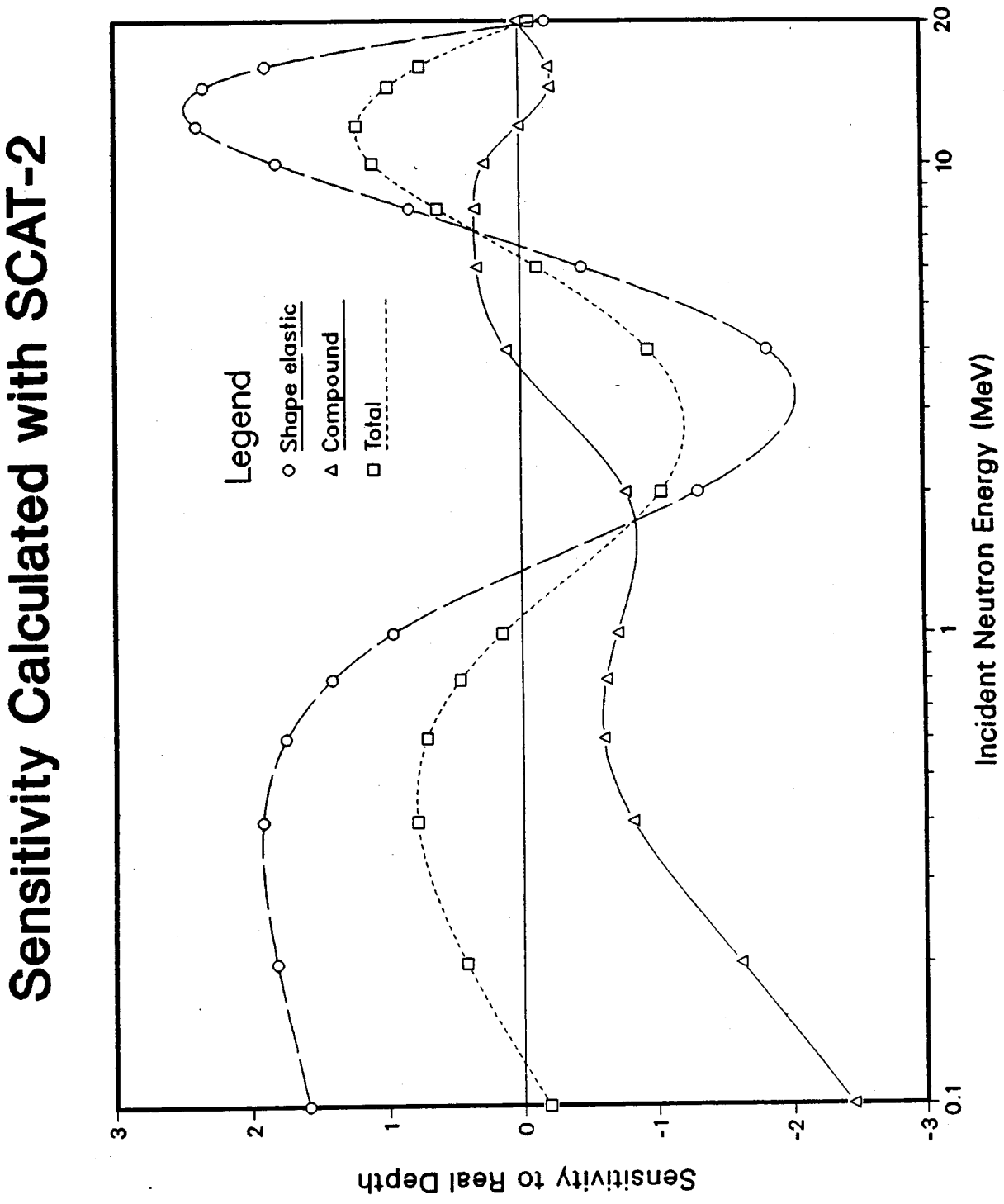

Fig. 11 Sensitivity of optical-model calculations to imaginary well depth obtained by SCAT-2

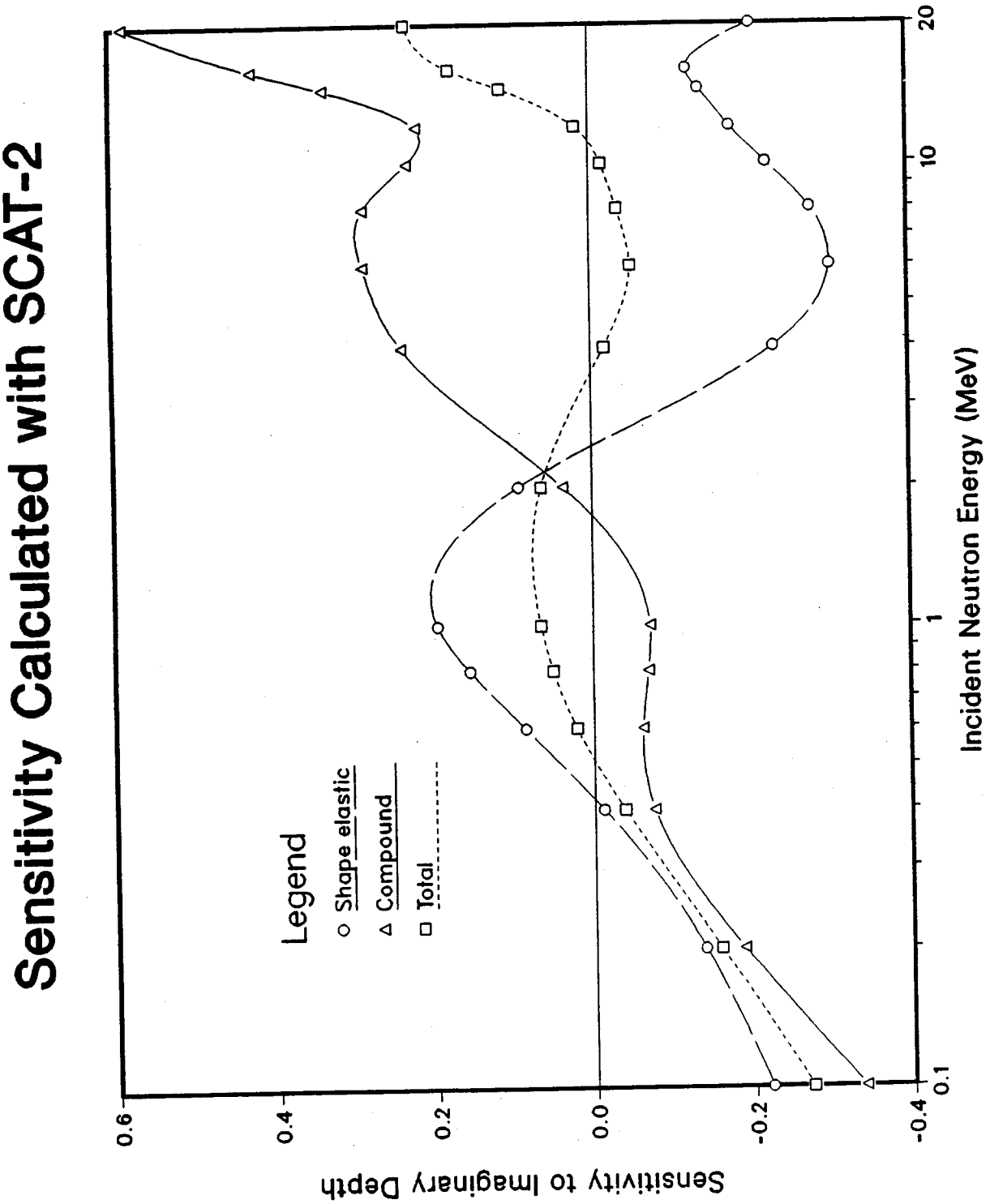

Fig. 12 Sensitivity of optical-model calculations to real radius obtained by SCAT-2

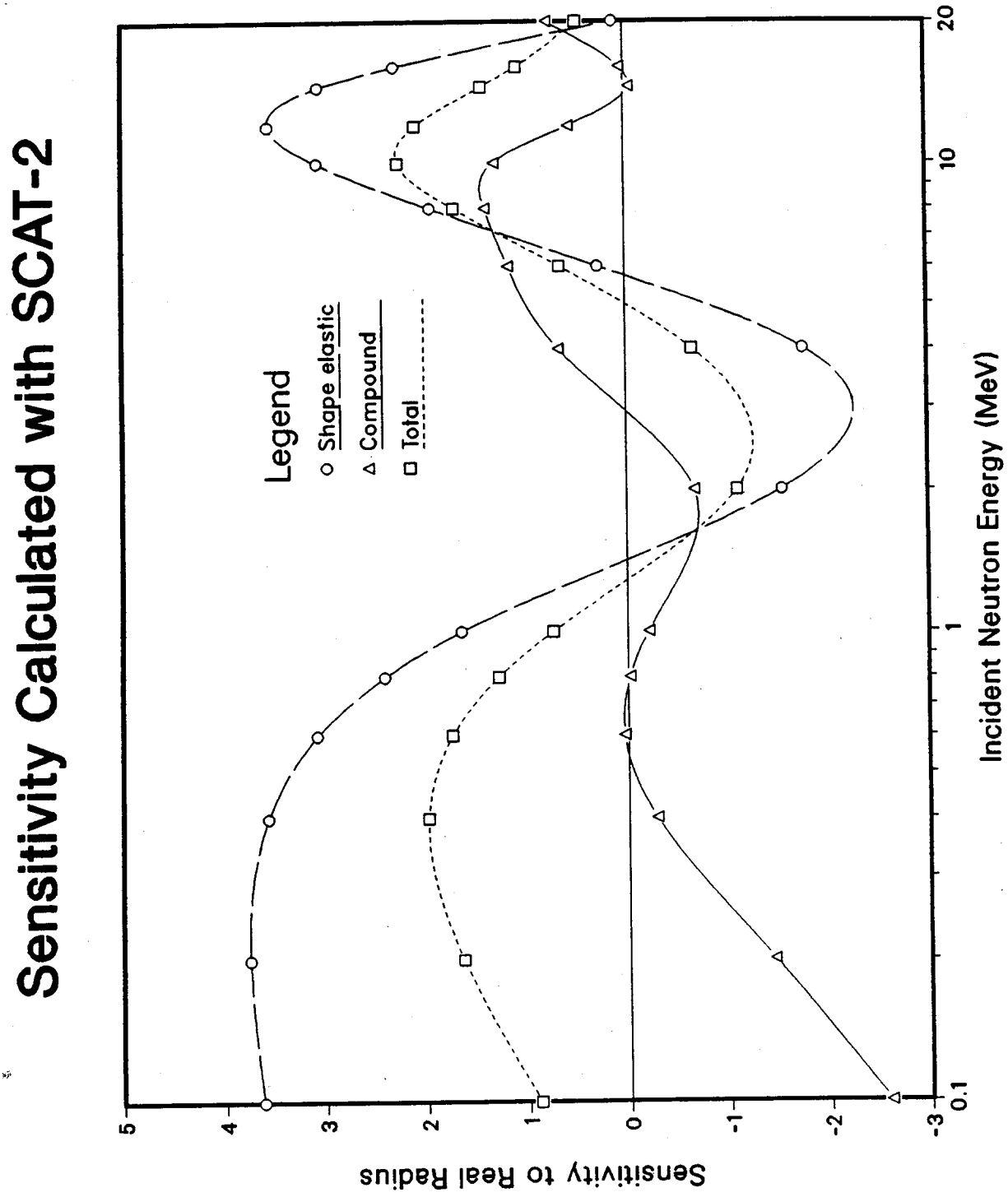

Fig. 13 Sensitivity of optical-model calculations to imaginary radius obtained by SCAT-2

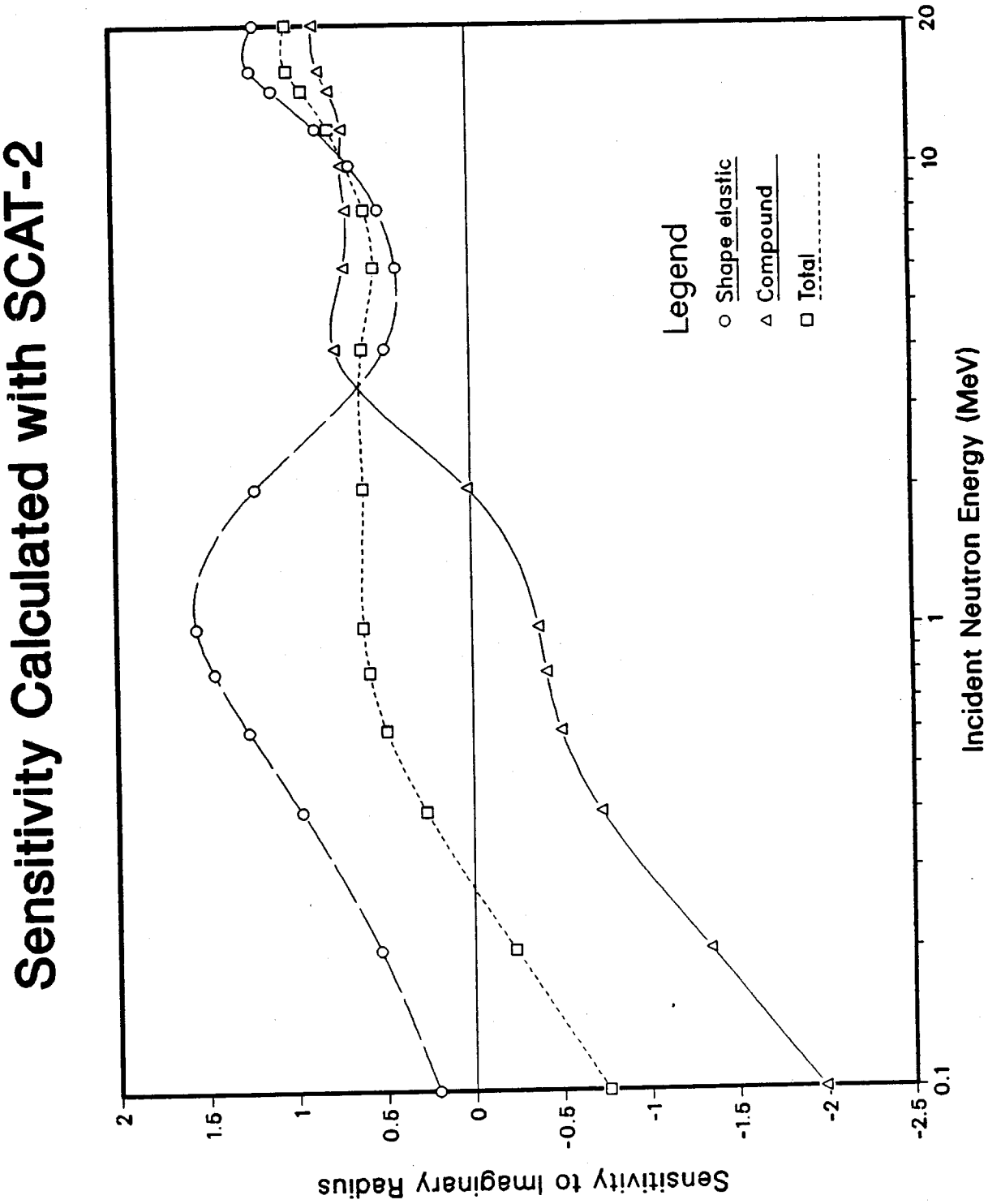

Fig. 14 Sensitivity of optical-model calculations to real diffuseness obtained by SCAT-2

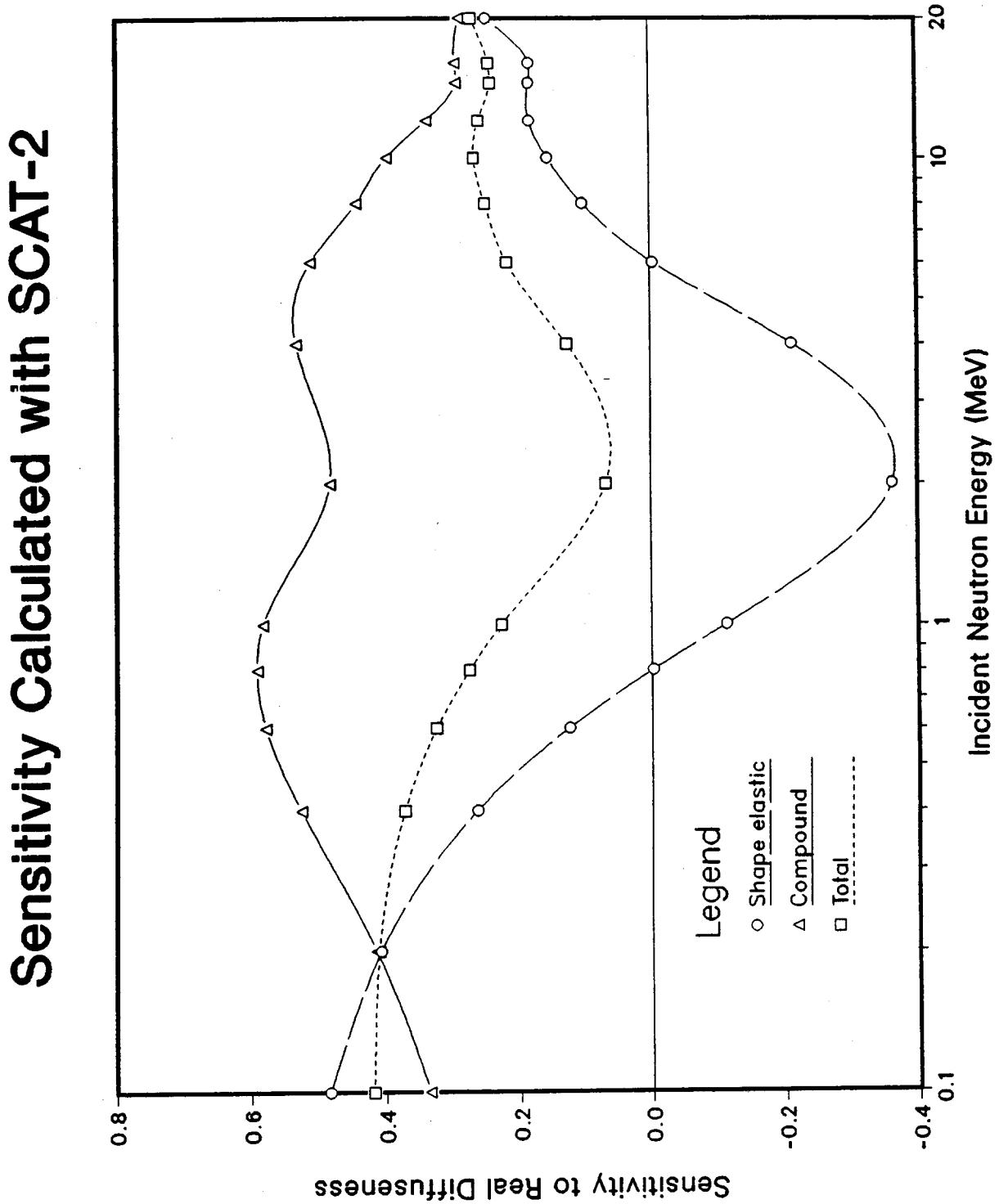

Fig. 15 Sensitivity of optical-model calculations to imaginary diffuseness obtained by SCAT-2

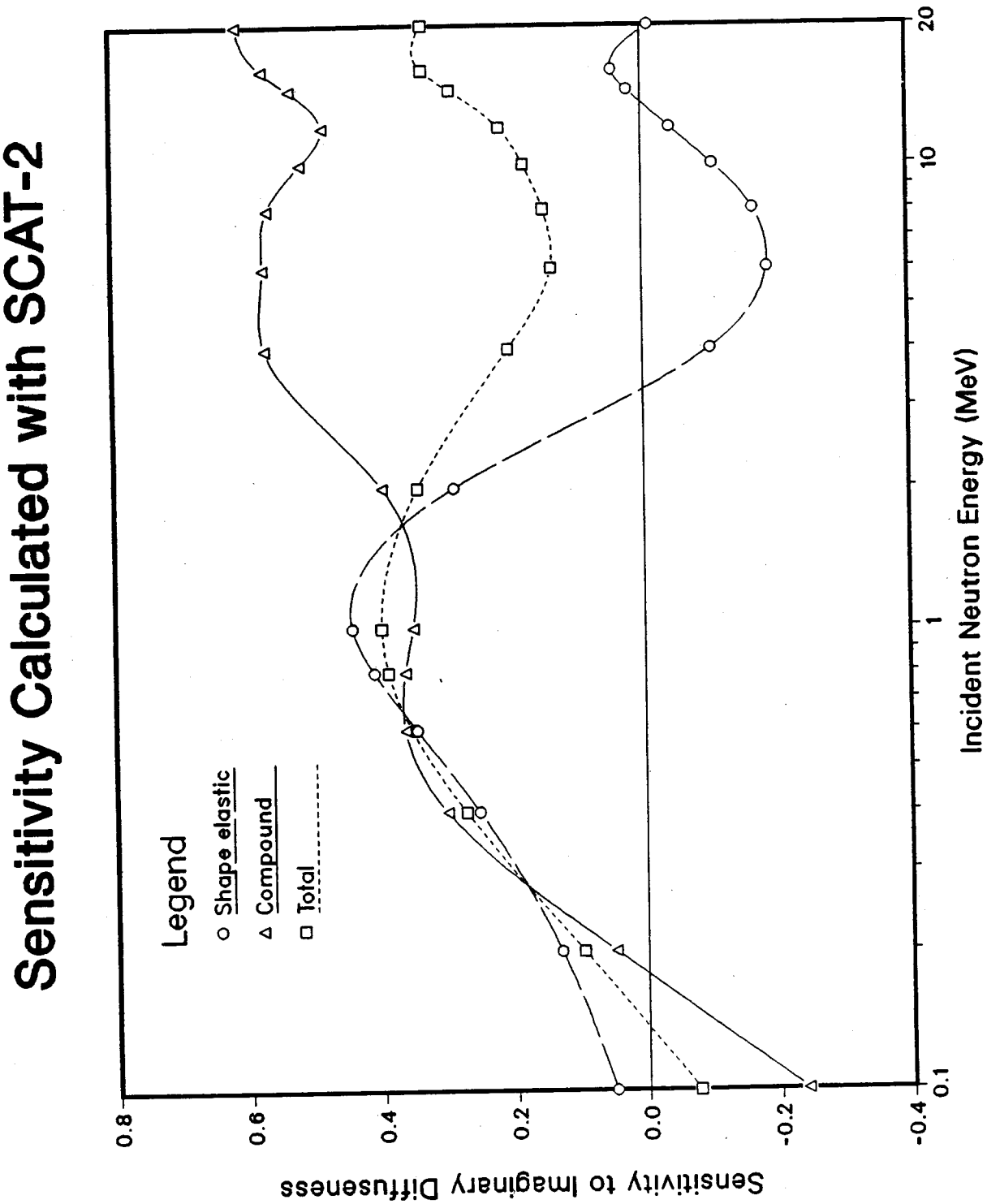

Fig. 16 Sensitivity of $^{56}Fe(n,n')$ reaction cross sections to optical model parameters

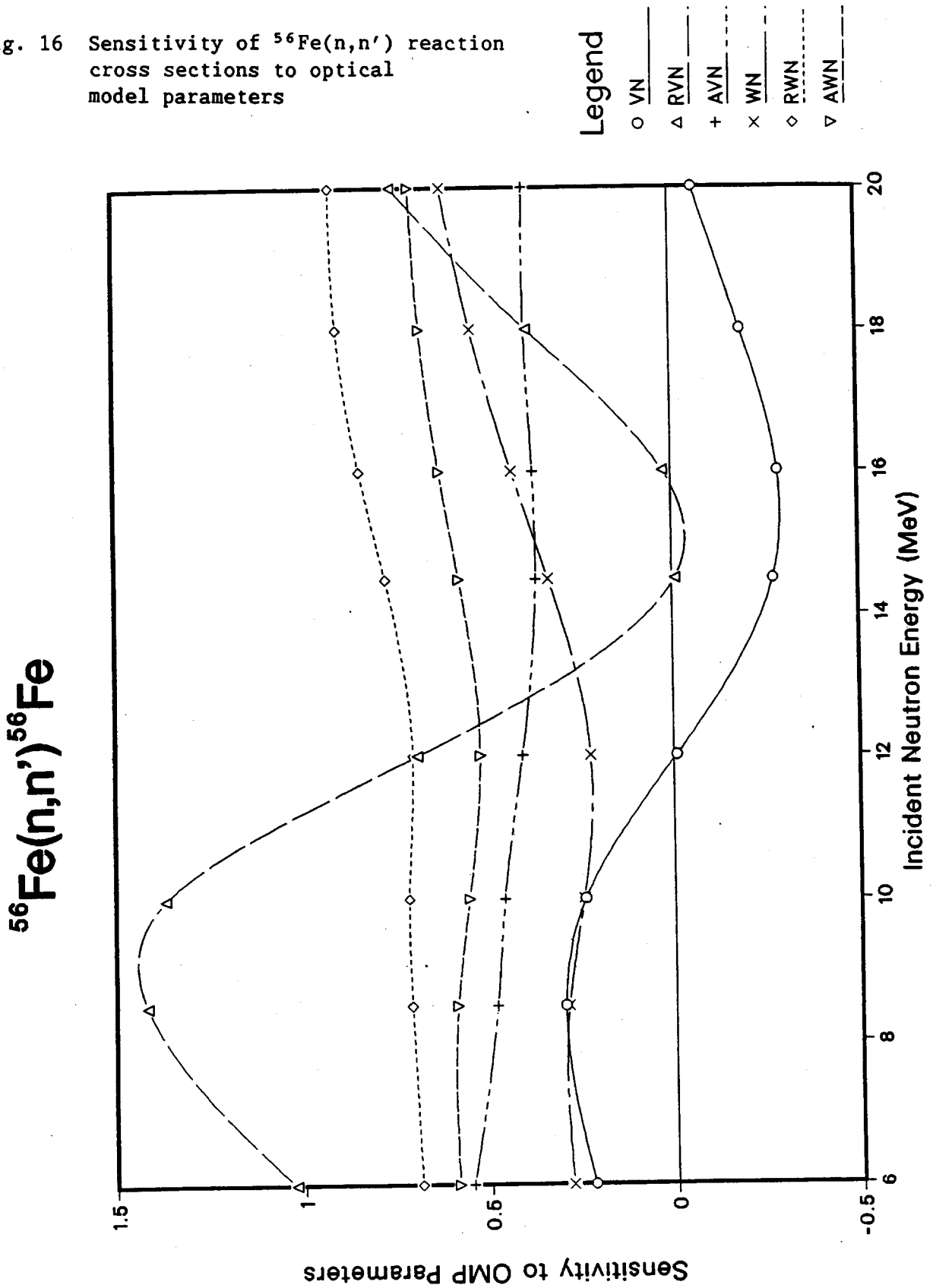

The symbols VN, RVN, AVN, WN, RWN and AWN stand for real depth, real radius, real diffuseness, imaginary depth, imaginary radius and imaginary diffuseness for neutron potentials, respectively.

Fig. 17 Sensitivity of $^{56}Fe(n,p)$ reaction cross sections to optical model parameters

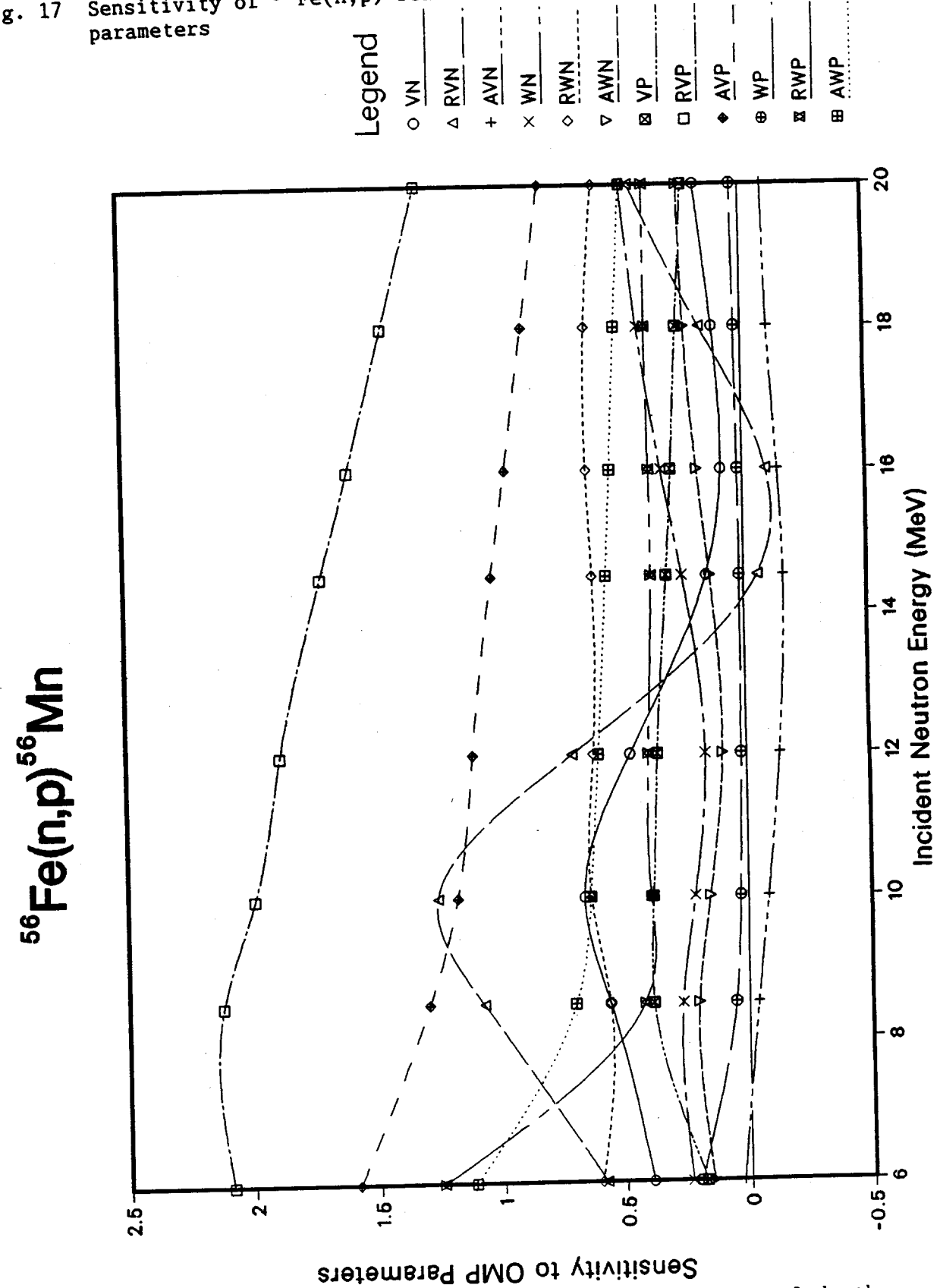

The symbols VP, RVP, AVP, WP, RWP and AWP stand for real depth, real radius, real diffuseness, imaginary depth, imaginary radius and imaginary diffuseness for proton potentials, respectively. For the remaining symbols, see the caption of Fig. 16.

Fig. 18 Sensitivity of $^{56}Fe(n,\alpha)$ reaction cross sections to optical model parameters

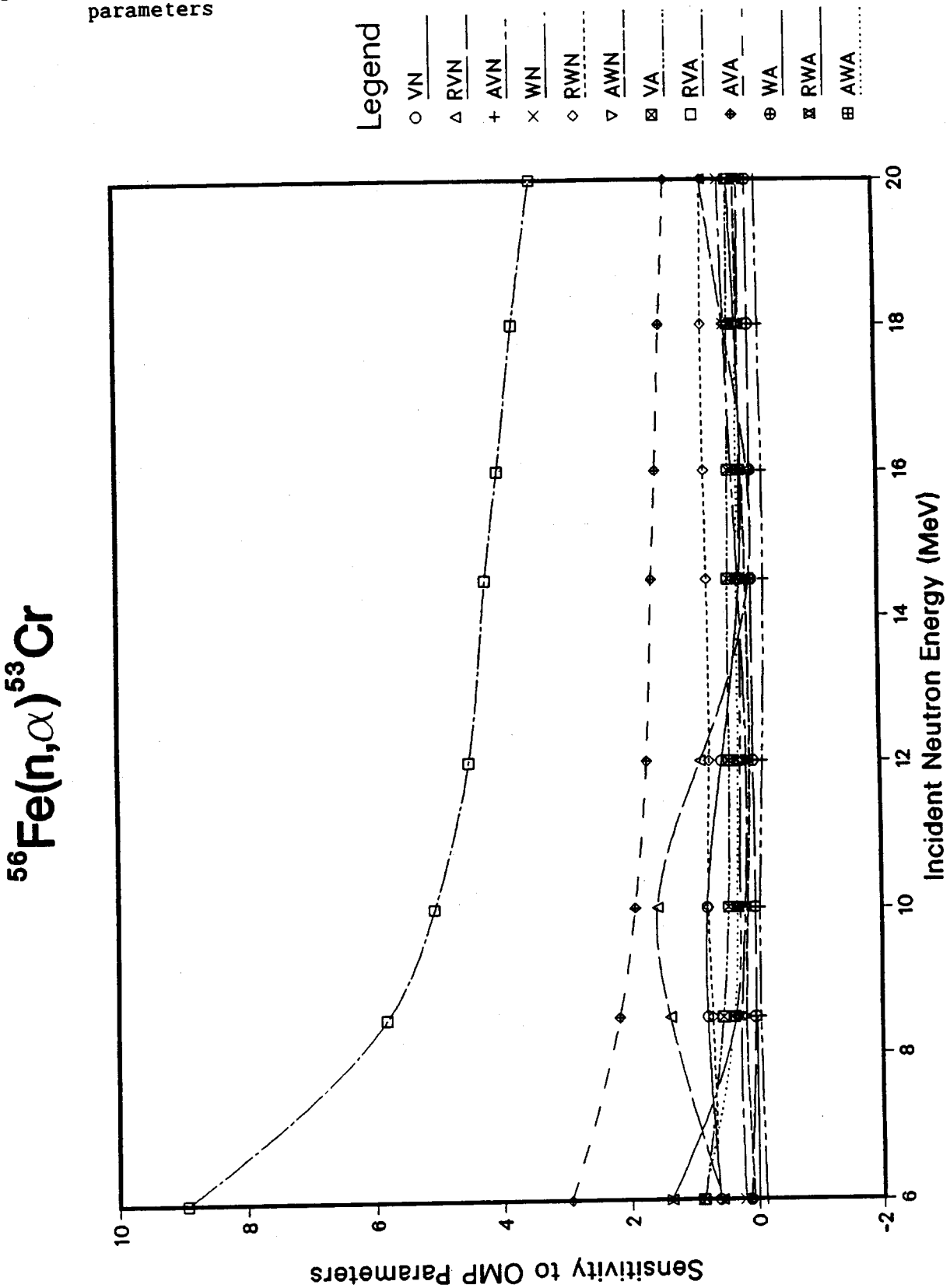

The symbols VA, RVA, AVA, WA, RWA and AWA stand for real depth, real radius, real diffuseness, imaginary depth, imaginary radius and imaginary diffuseness for α-particle potentials, respectively. For the remaining symbols, see the caption of Fig. 16.

Fig. 19 Sensitivity of $^{56}Fe(n,n')$ reaction cross section to level density parameters

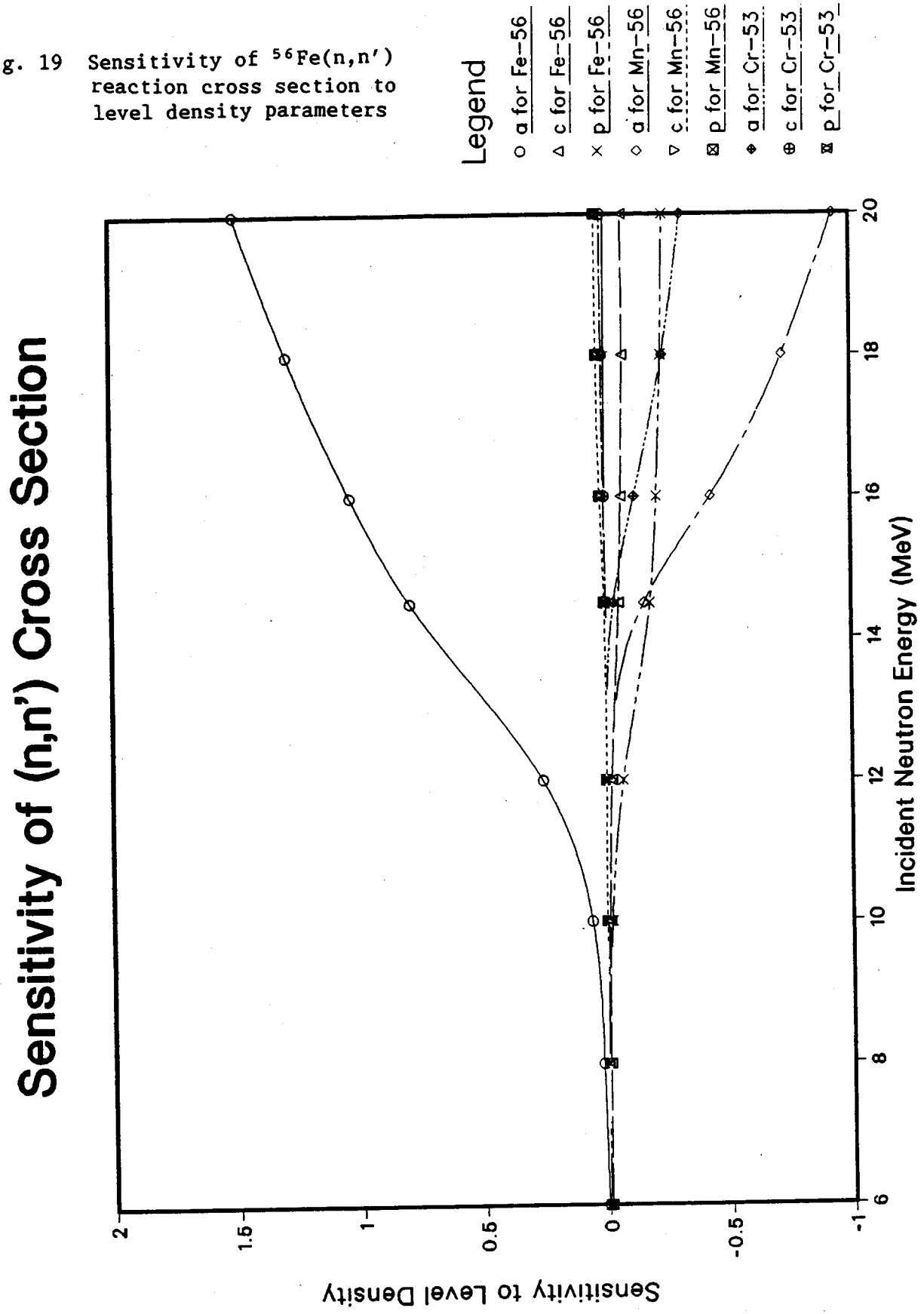

The symbols a, c and p stand for a, spin cut-off and pairing energy correction parameters.

Fig. 20 Sensitivity of $^{56}Fe(n,p)$ reaction cross sections to level density parameters

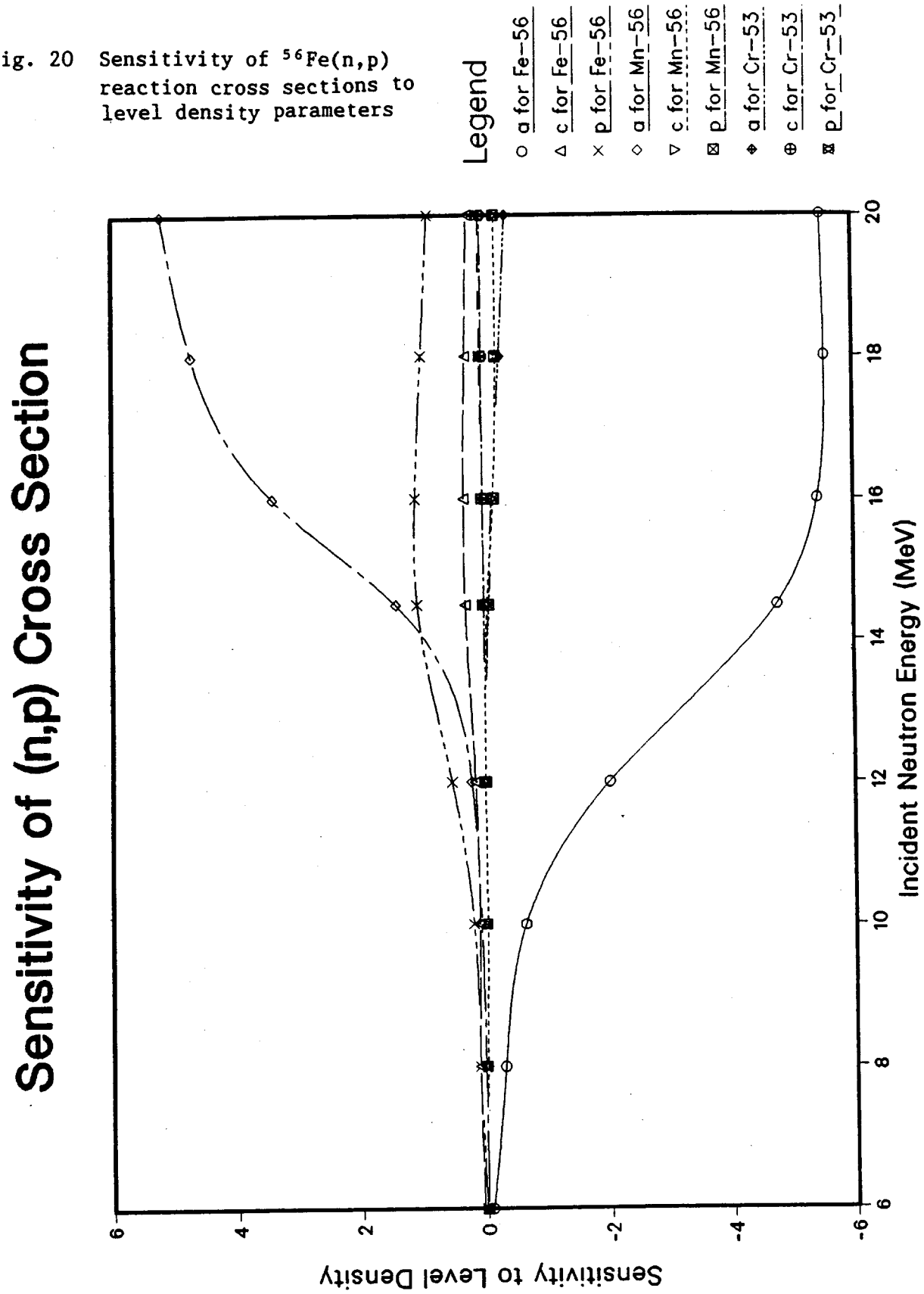

The symbols a, c and p stand for a, spin cut-off and pairing energy correction parameters.

Fig. 21 Sensitivity of $^{56}Fe(n,\alpha)$ reaction cross sections to level density parameters

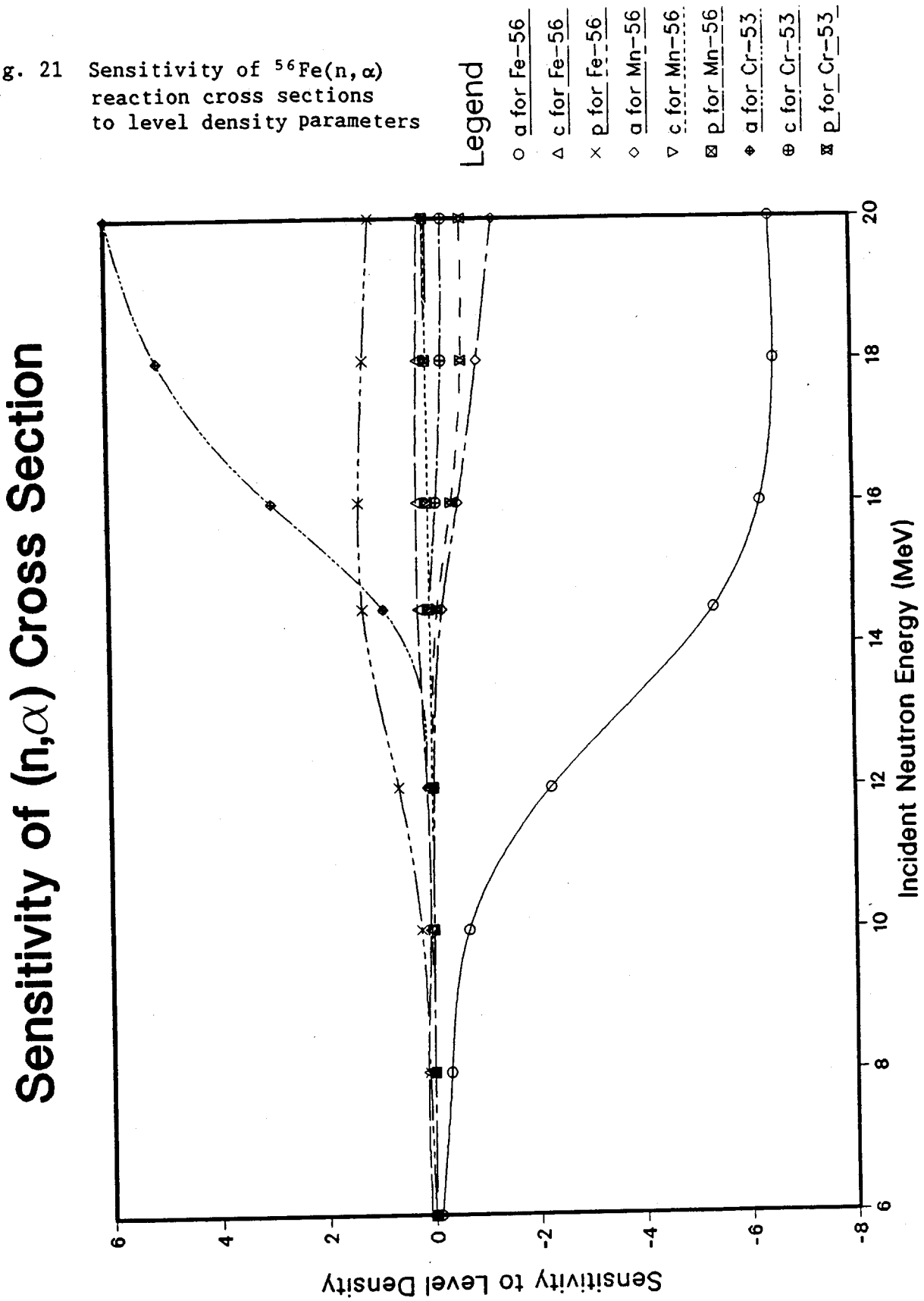

The symbols a, c and p stand for a, spin cut-off and pairing energy correction parameters.

Fig. 22 Sensitivity of (n,n'), (n,p) and (n,α) reaction cross sections to precompound parameter

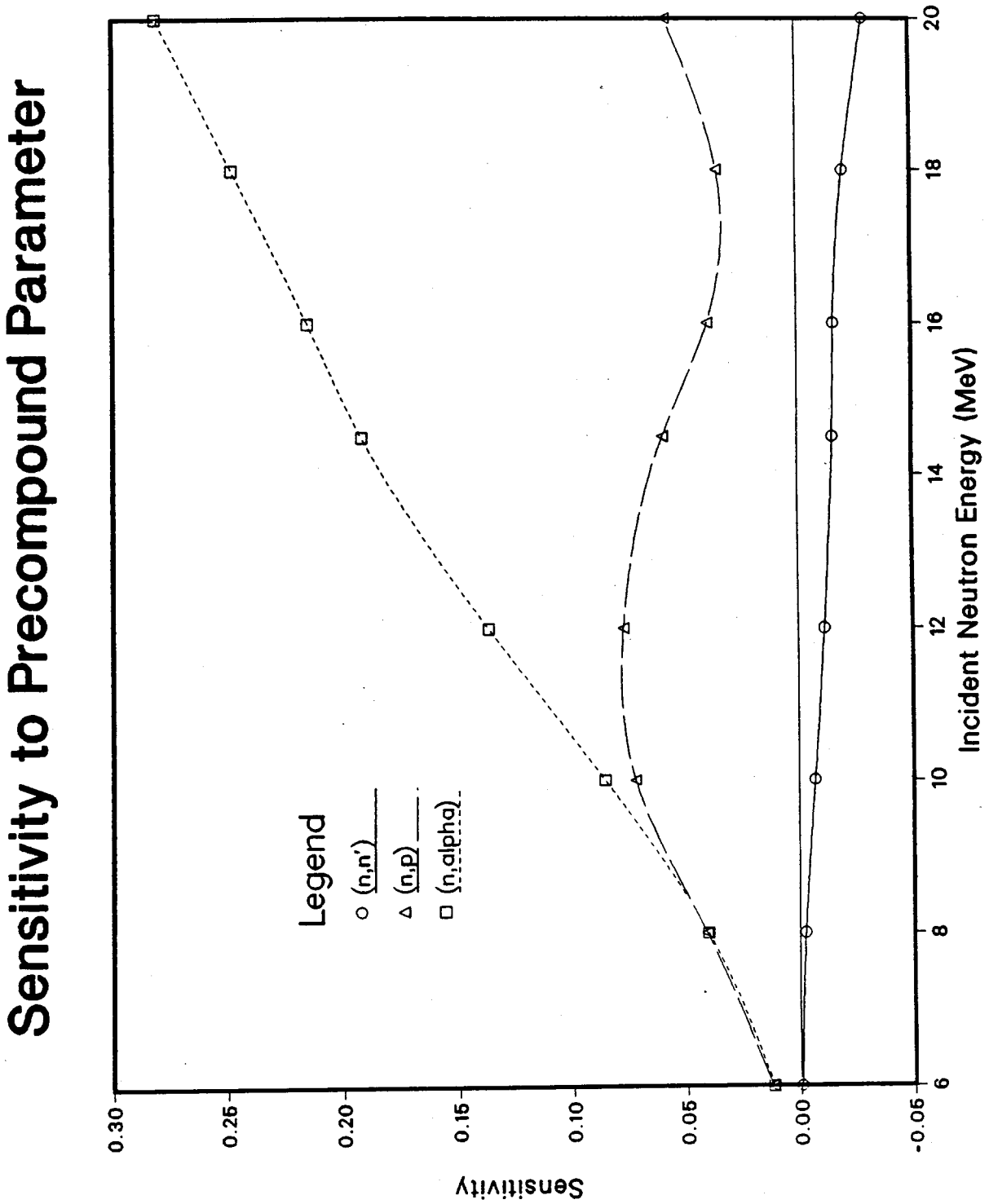

Fig. 23 Sensitivity of continuum neutron spectrum at 14.5 MeV to precompound parameter

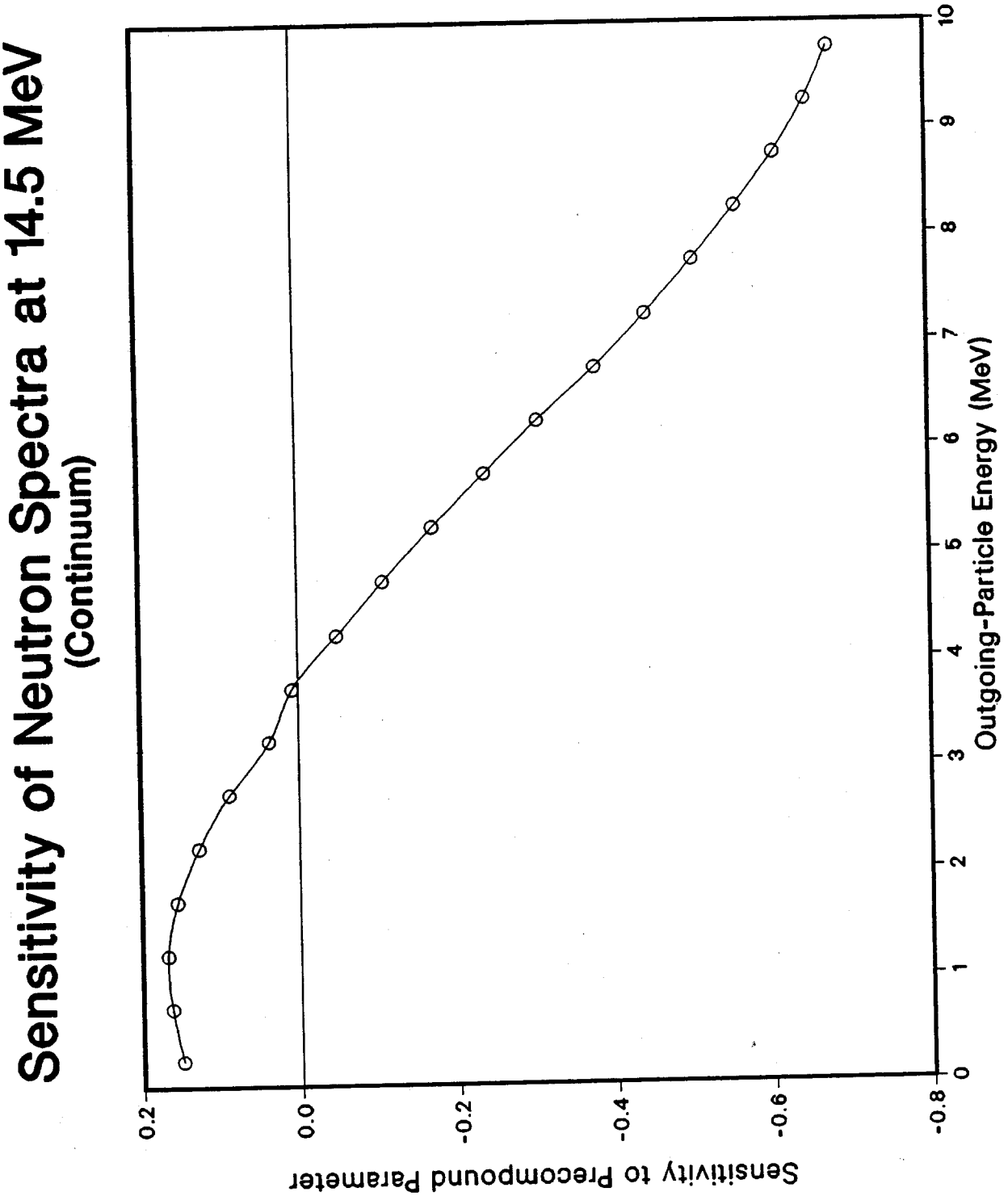

Fig. 24 Sensitivity of $^{56}Fe(n,nx)$ reaction cross sections to giant dipole resonance parameters

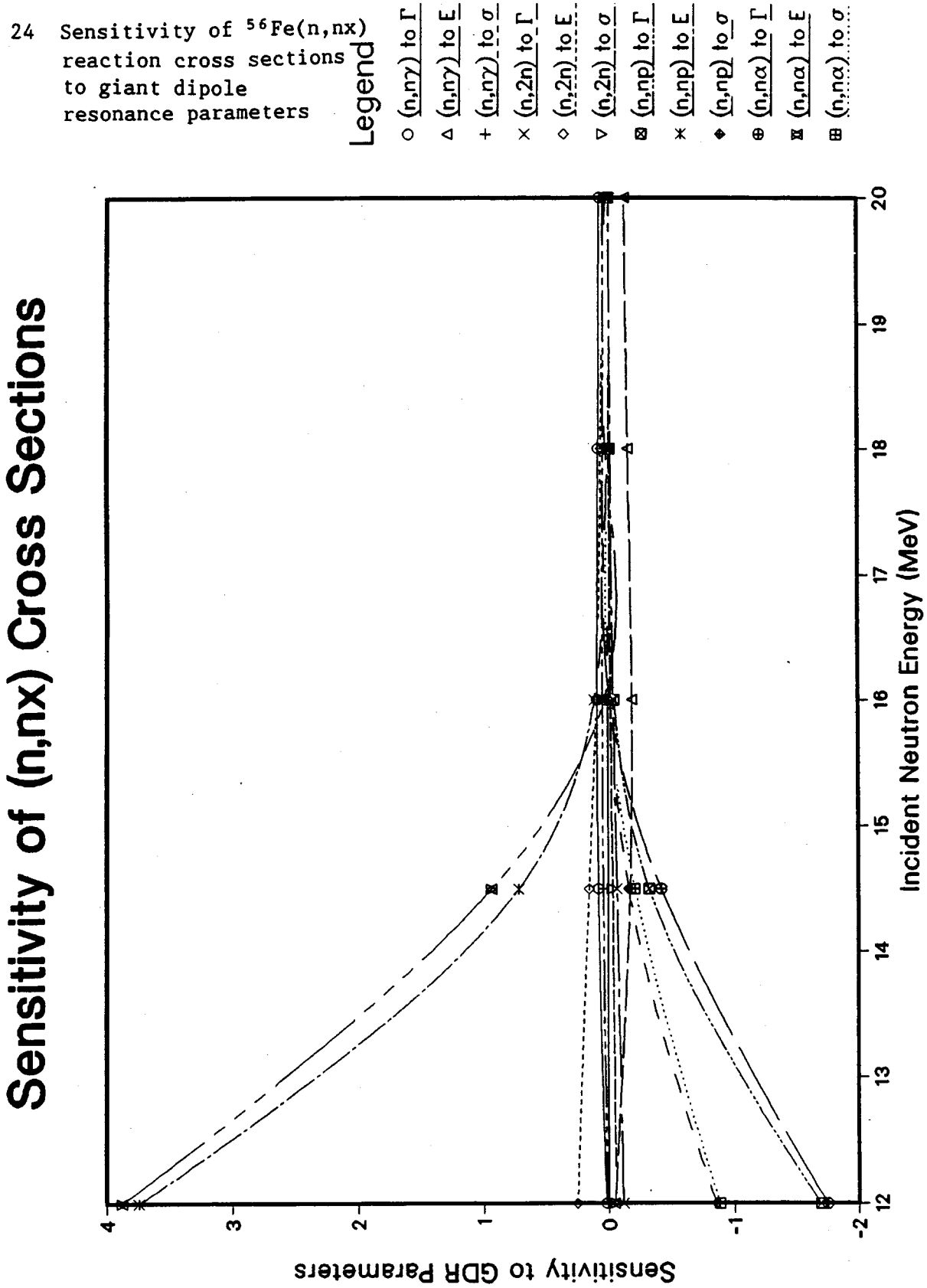

Fig. 25 Sensitivity of $^{56}Fe(n,px)$ reaction cross sections to giant dipole resonance parameters

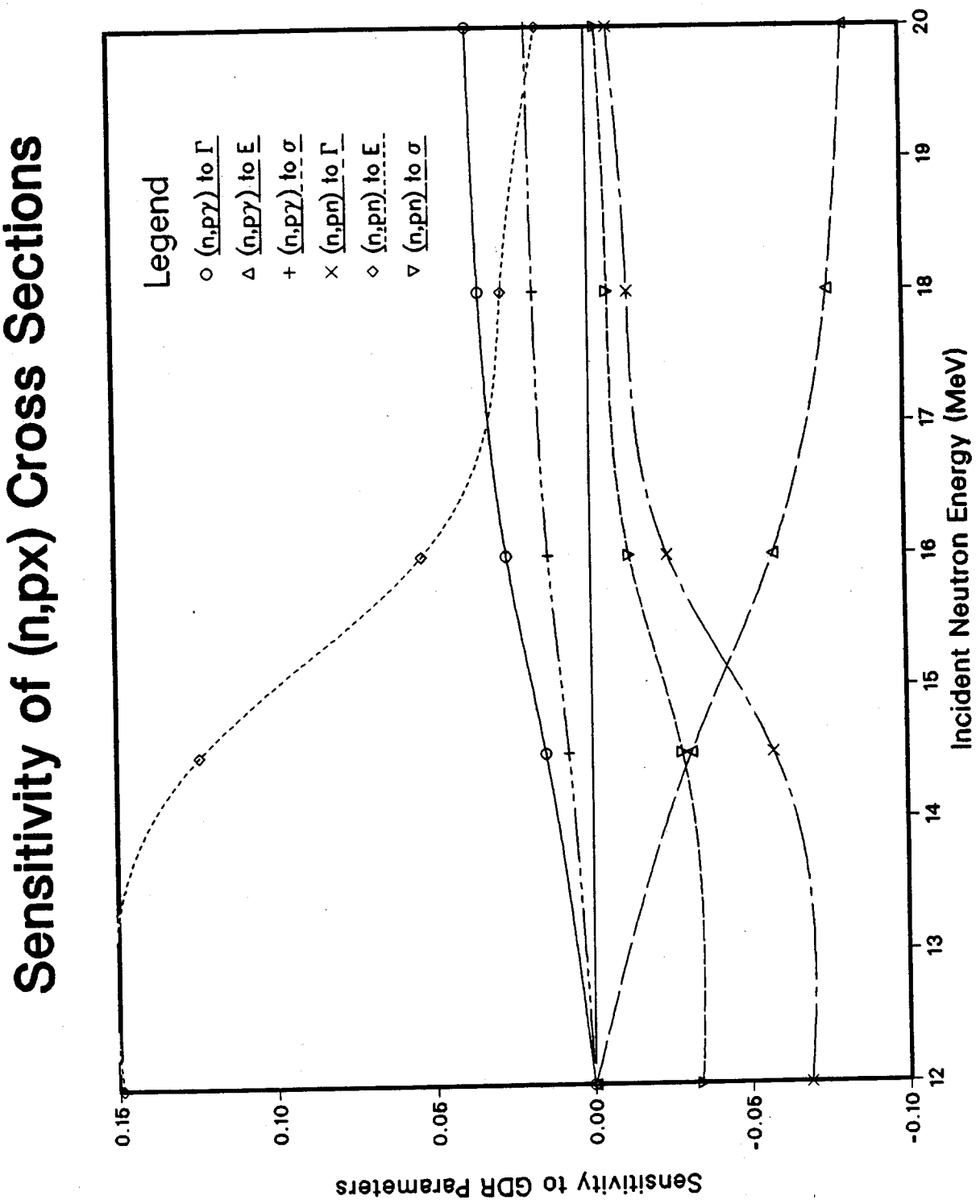

Fig. 26 Sensitivity of $^{56}Fe(n,\alpha x)$ reaction cross sections to giant dipole resonance parameters

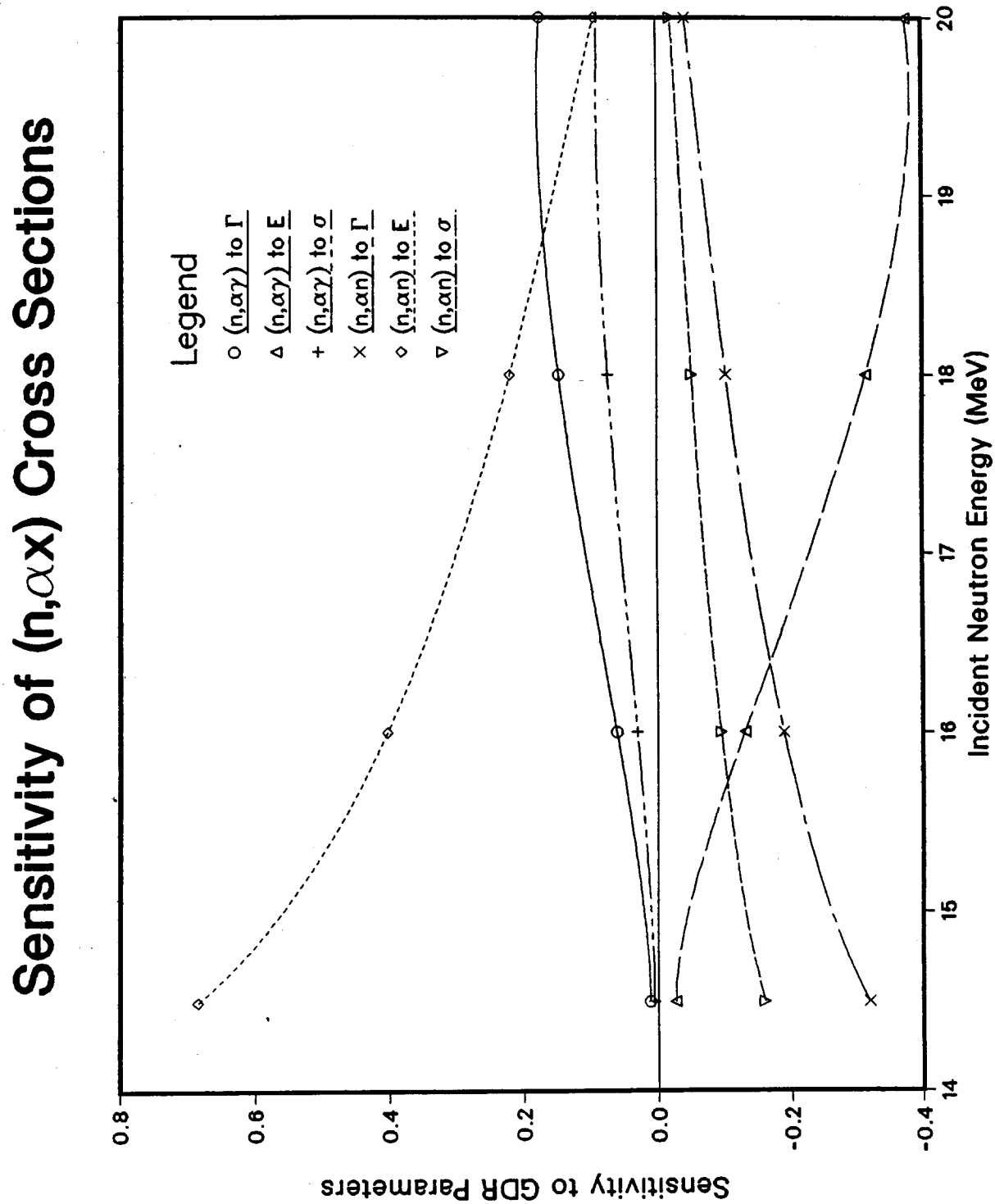

Fig. 27 Neutron emission spectrum at 14.5 MeV
Uncertainty of ±1% was assumed for the real radius of the neutron potentials.

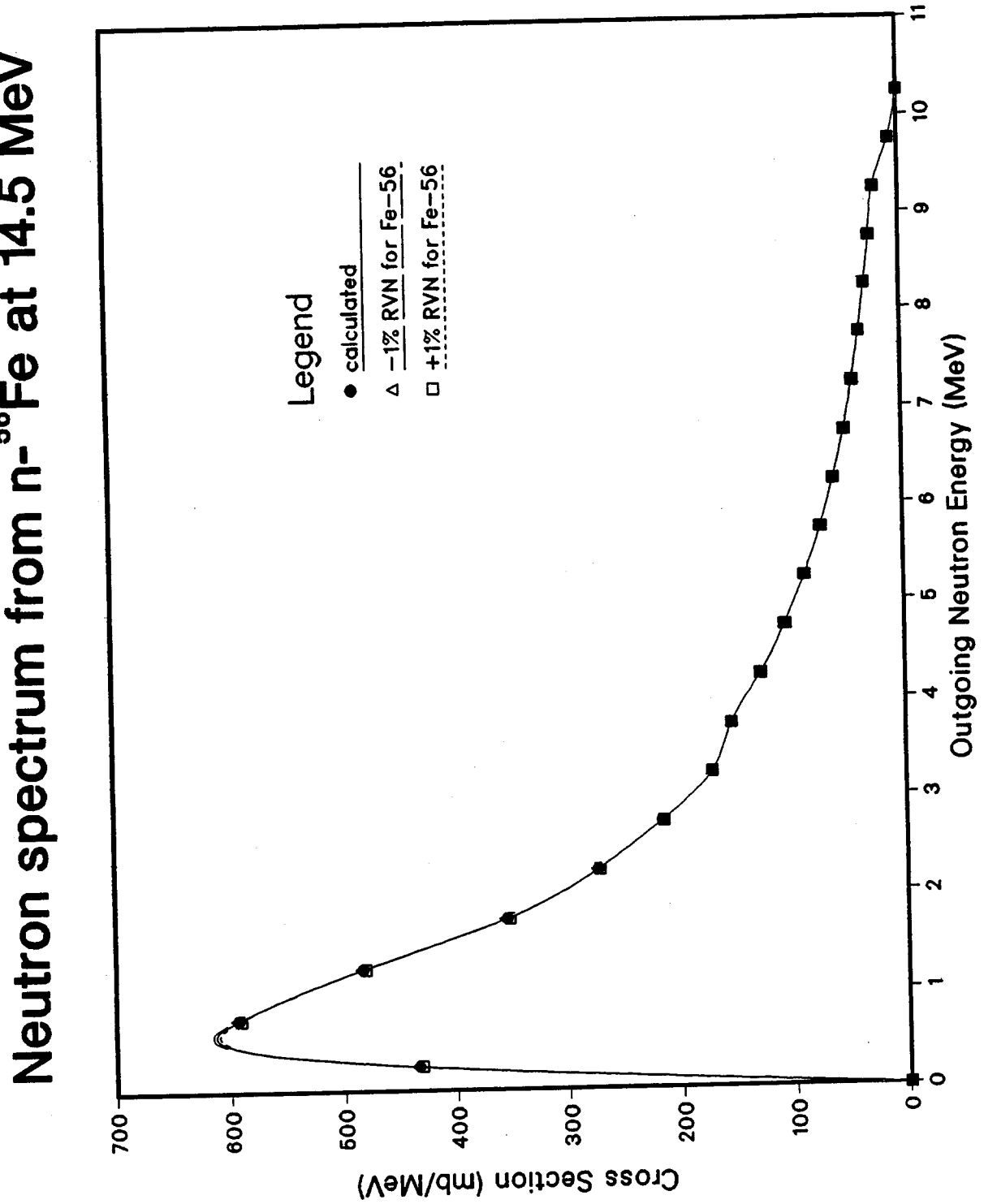

Fig. 28 Proton emission spectrum at 14.5 MeV
Uncertainty of ±1% was assumed for the real radius of the proton potentials.

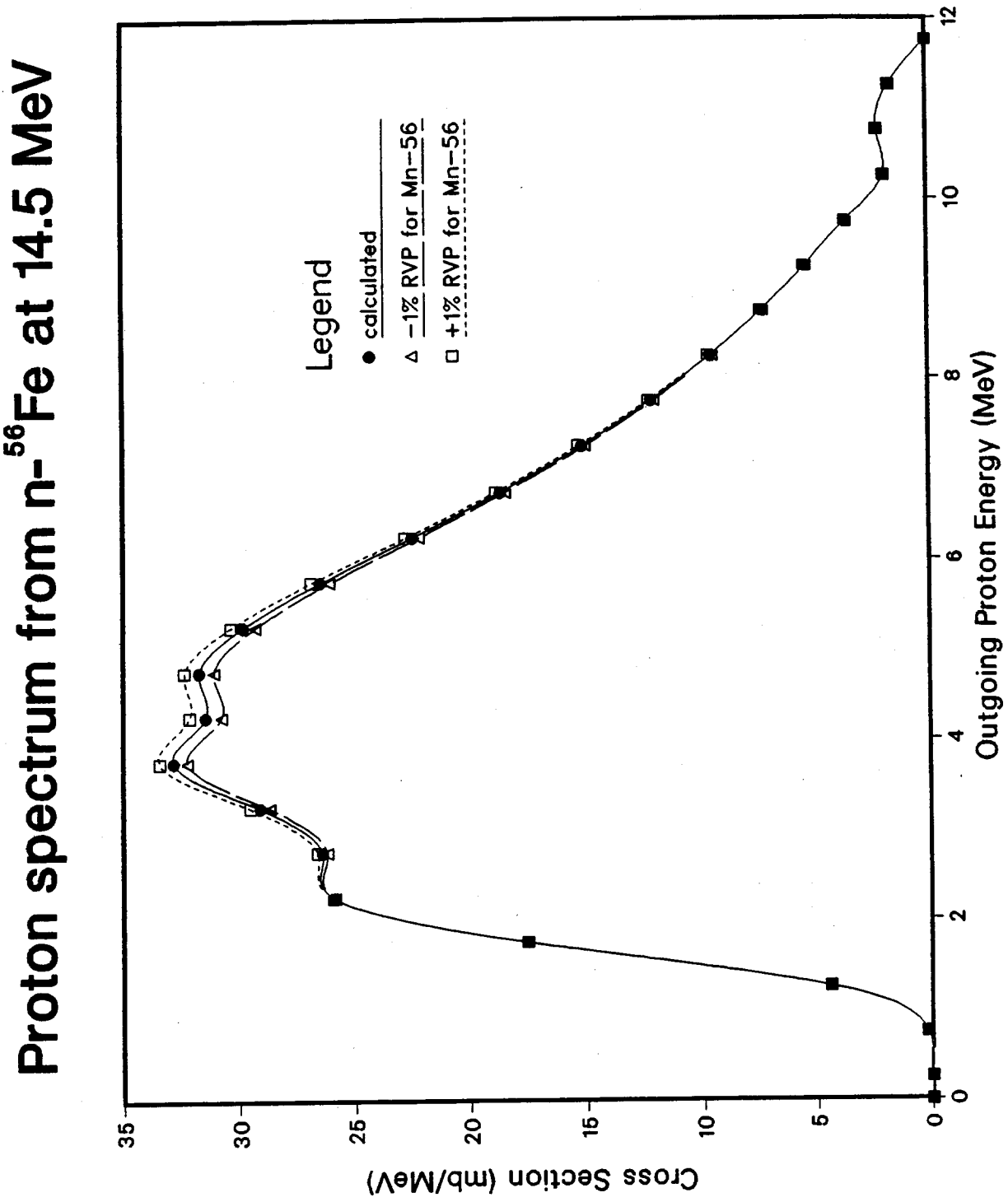

Fig. 29 α-particle emission spectrum at 14.5 MeV
Uncertainty of ±1% was assumed for the real radius of the α-particle potentials.

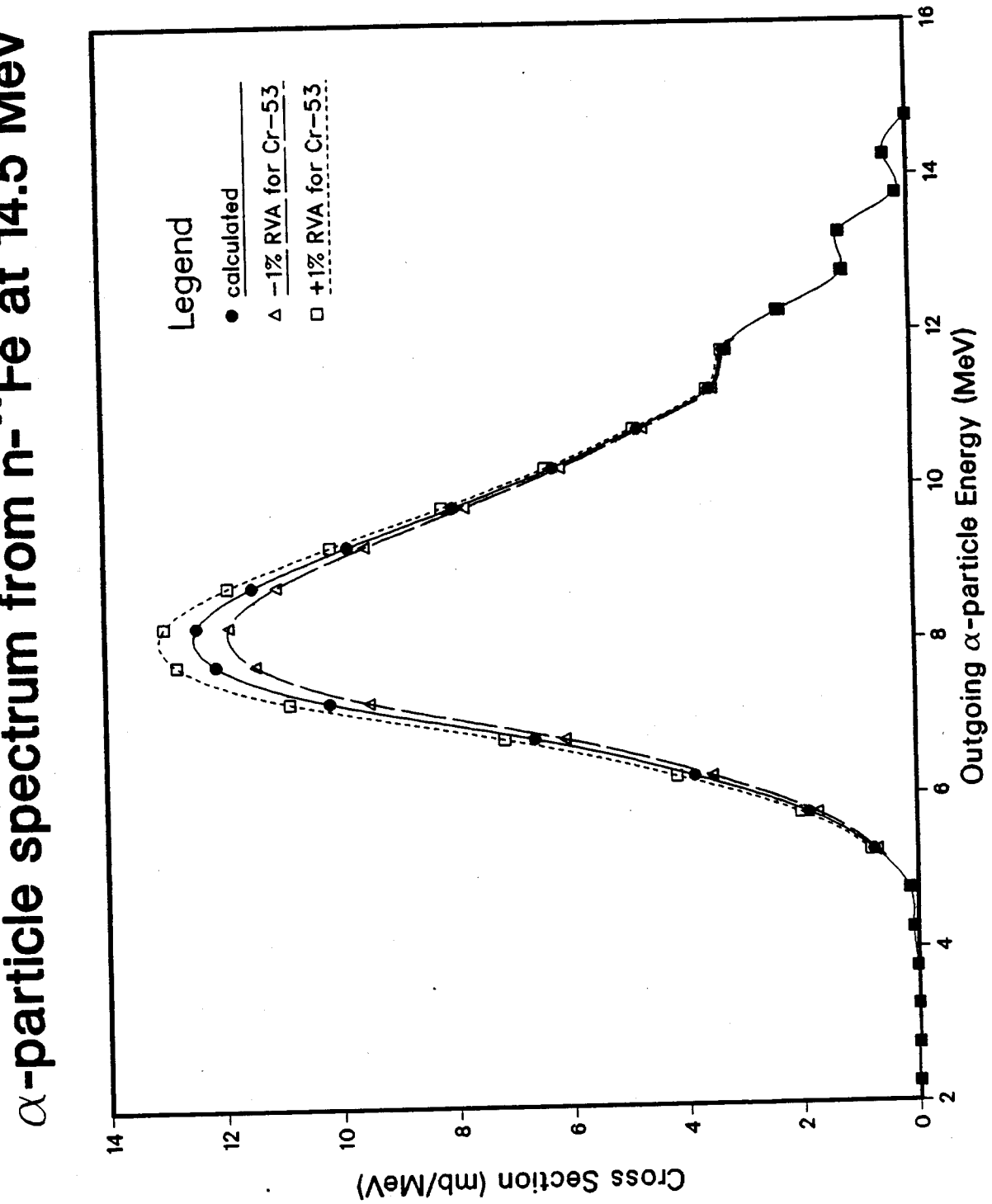

Fig. 30 $^{56}Fe(n,n\gamma)$ reaction cross section
Uncertainty of ±1% was assumed for the a parameter for ^{56}Fe.

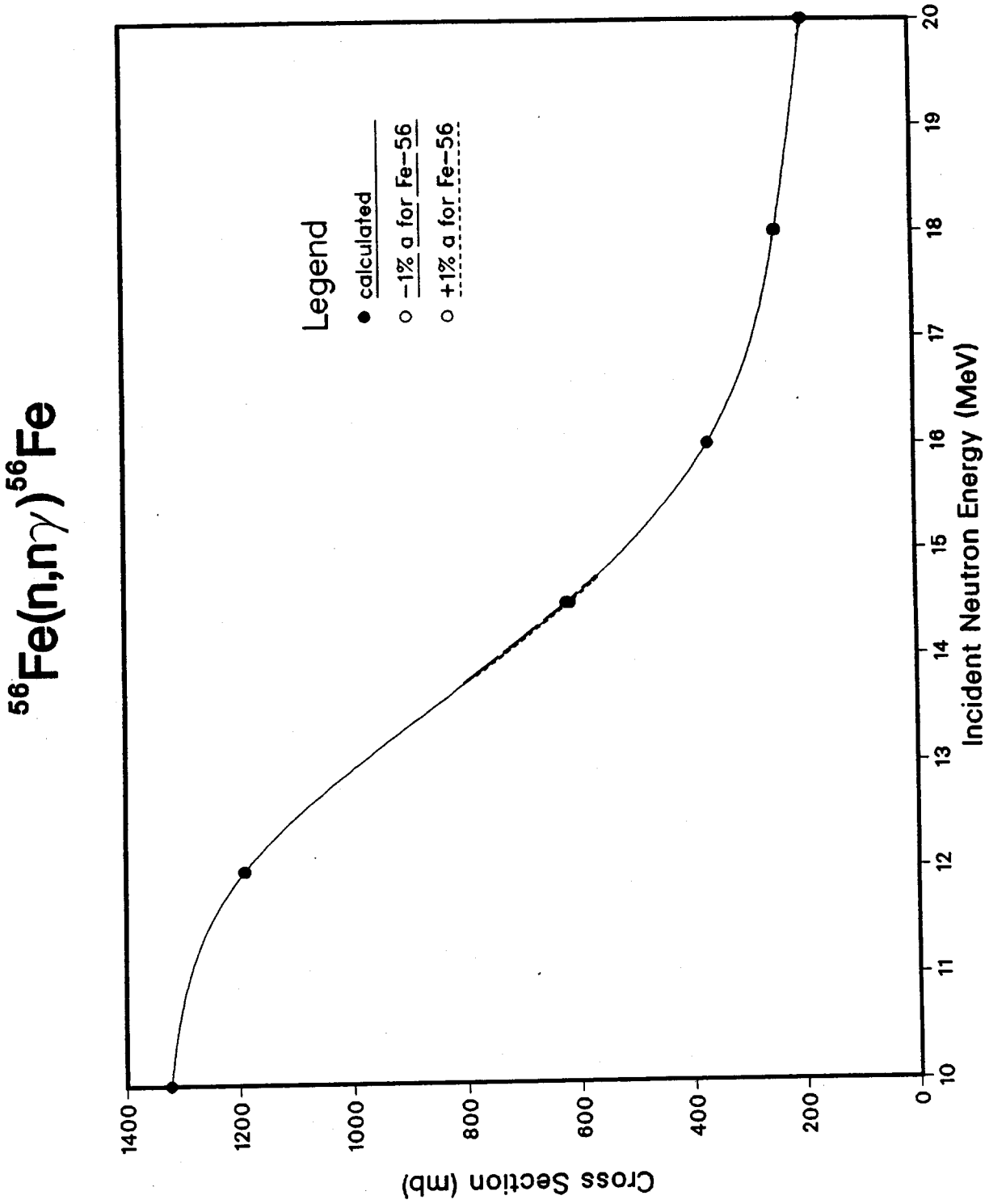

Fig. 31 $^{56}Fe(n,2n)$ reaction cross section
Uncertainty of ±1% was assumed for the a parameter for ^{56}Fe.

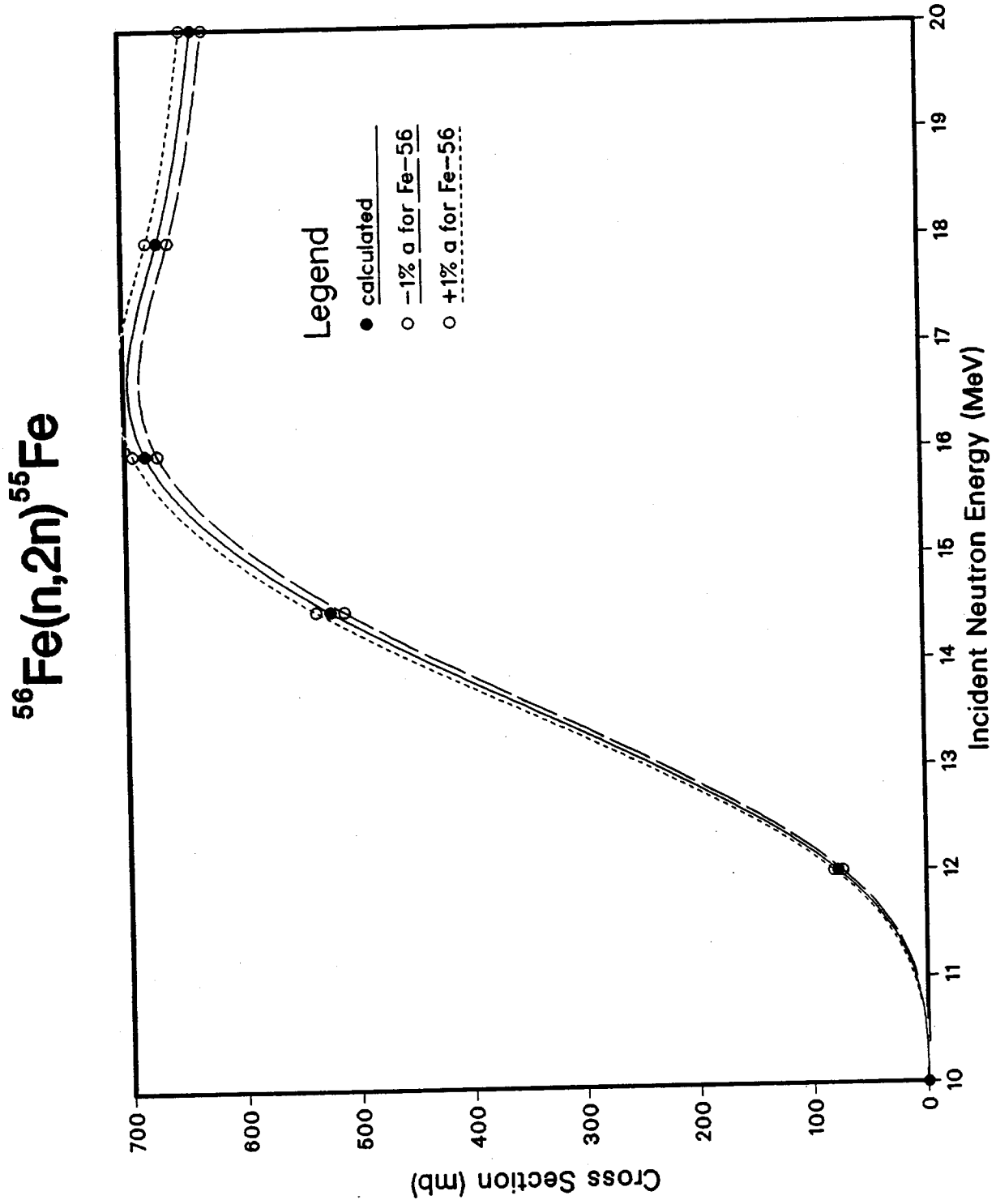

Fig. 32 ^{56}Fe(n,np) reaction cross section
Uncertainty of ±1% was assumed for the a parameter for ^{56}Fe.

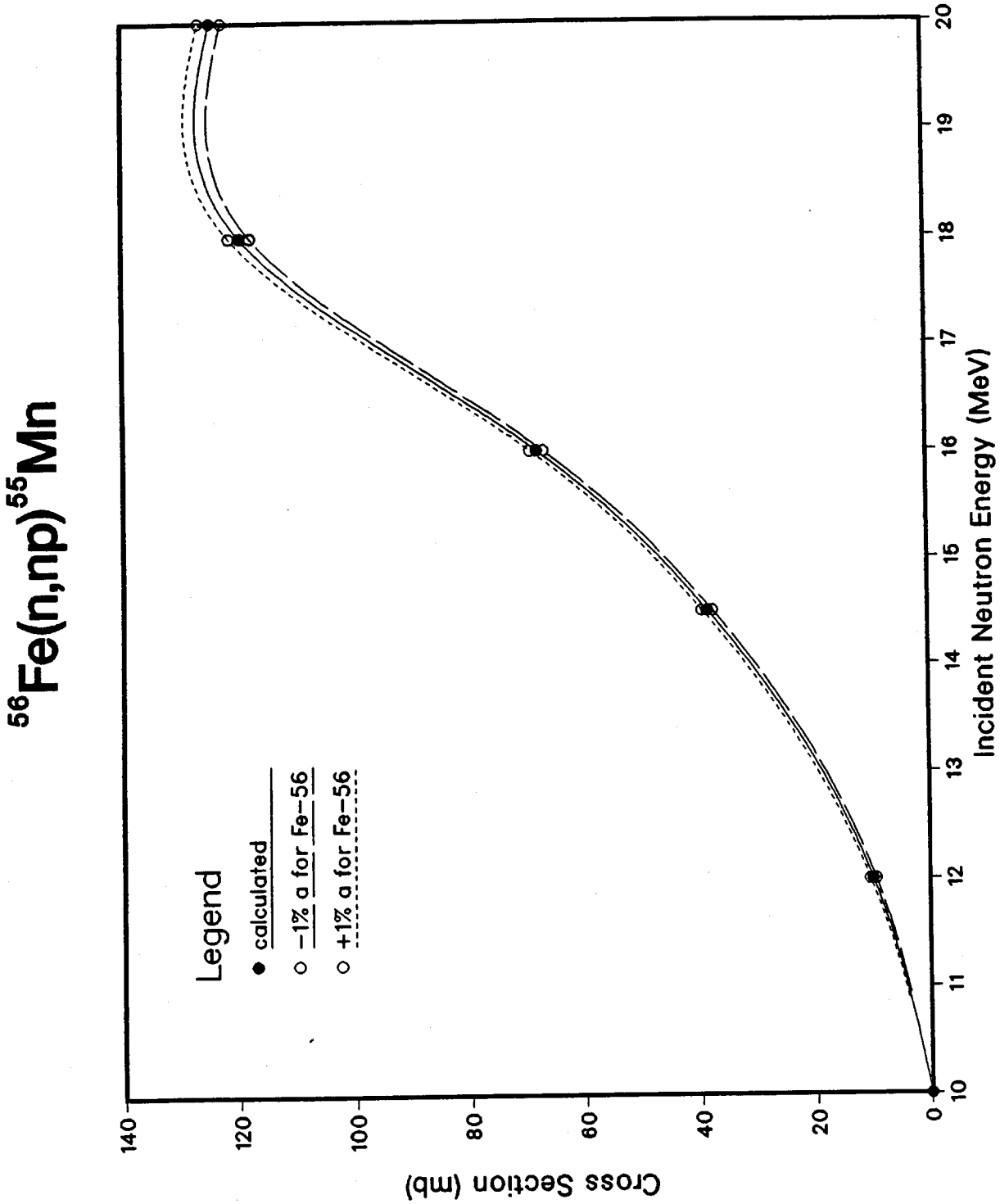

Fig. 33 $^{56}Fe(n,n\alpha)$ reaction cross section
Uncertainty of ±1% was assumed for the a parameter for ^{56}Fe.

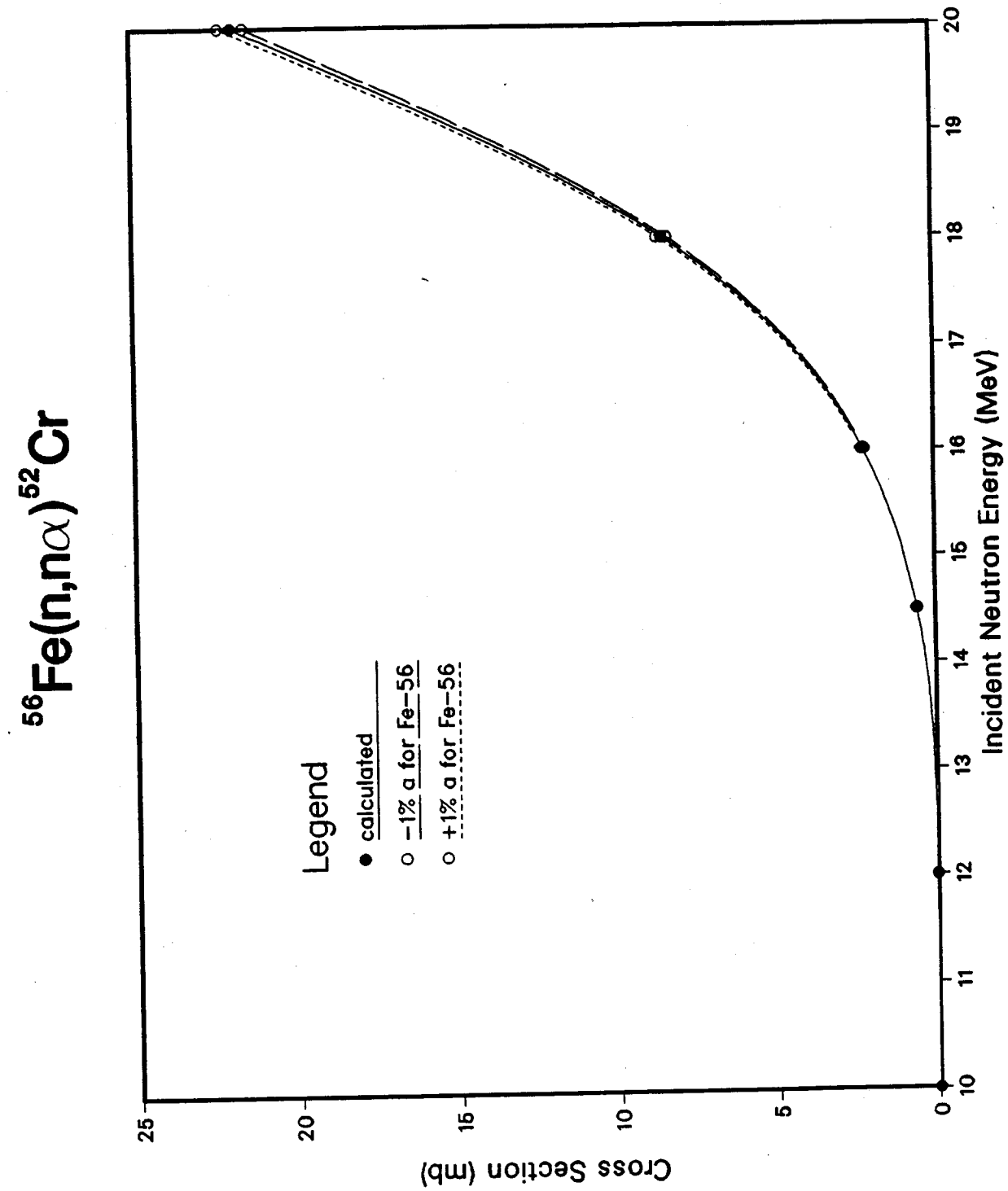

Fig. 34 $^{56}Fe(n,p\gamma)$ reaction cross section
Uncertainty of ±1% was assumed for the a parameter for ^{56}Fe.

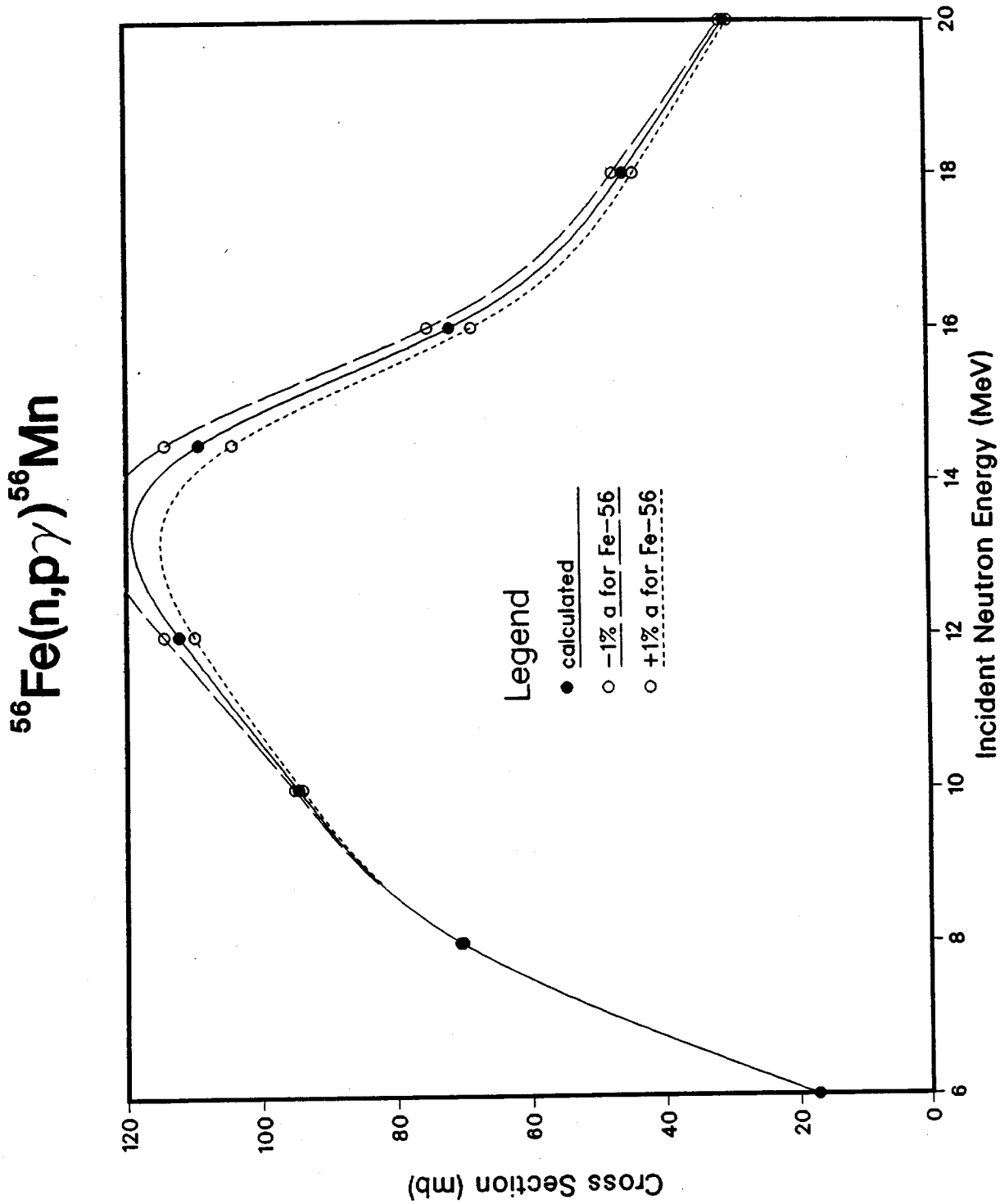

Fig. 35 ^{56}Fe(n,pn) reaction cross section
Uncertainty of ±1% was assumed for the a parameter for ^{56}Fe.

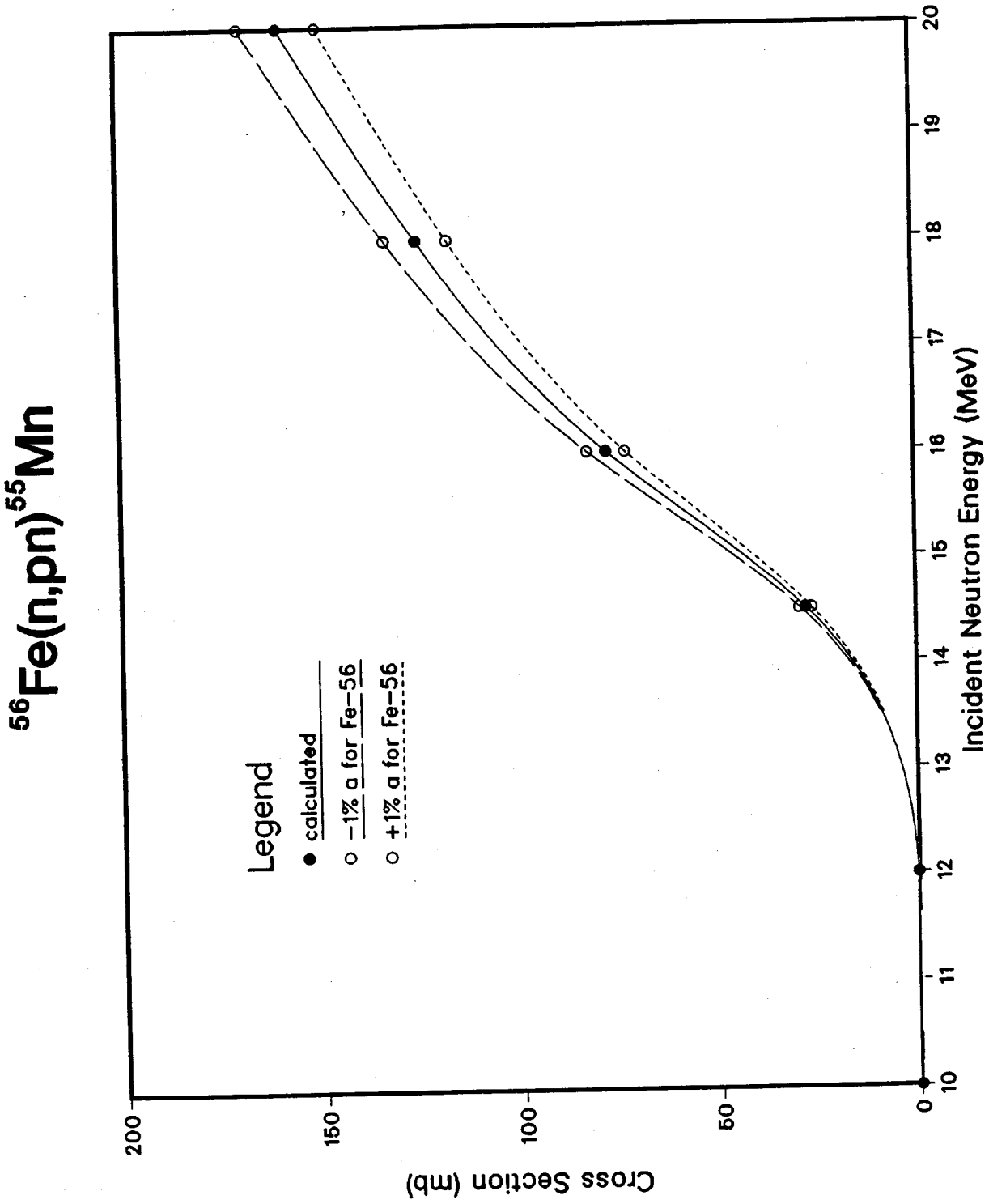

Fig. 36 $^{56}Fe(n,\alpha\gamma)$ reaction cross section
Uncertainty of ±1% was assumed for the a parameter for ^{56}Fe.

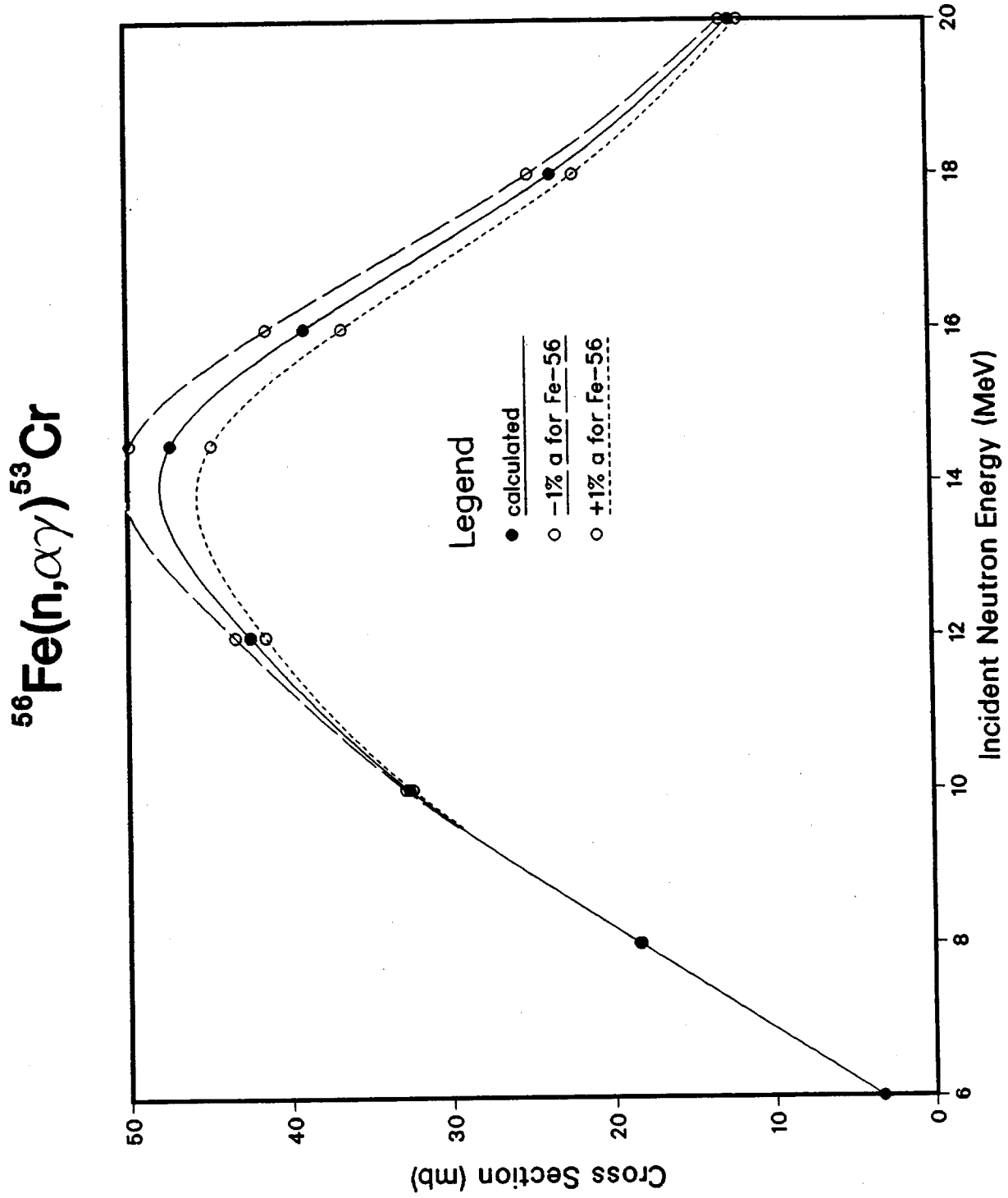

Fig. 37 $^{56}Fe(n,\alpha n)$ reaction cross section
Uncertainty of ±1% was assumed for the a parameter for ^{56}Fe.

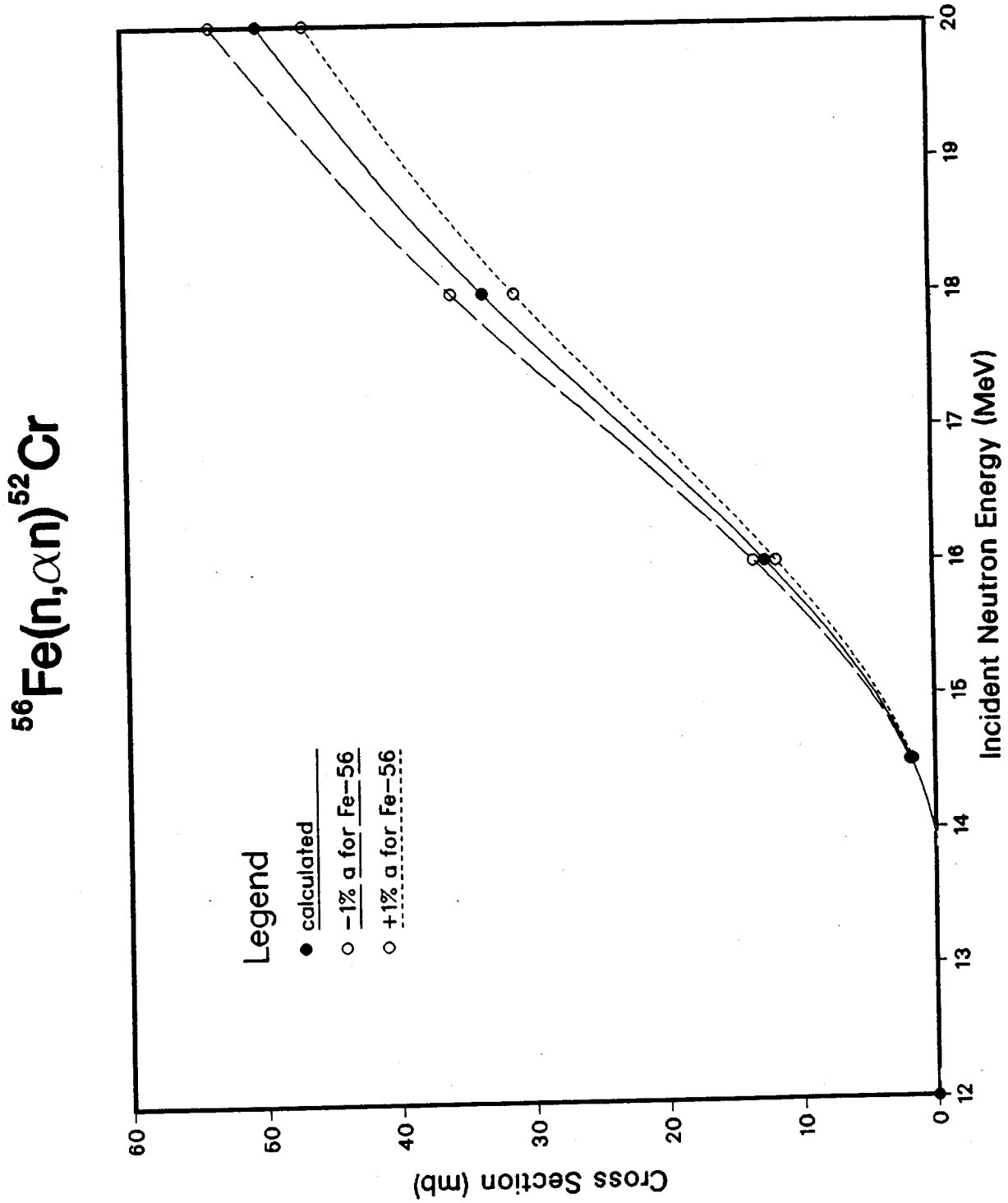

Fig. 38 Neutron emission spectrum at 14.5 MeV
Uncertainty of ±1% was assumed for the a parameter for ^{56}Fe.

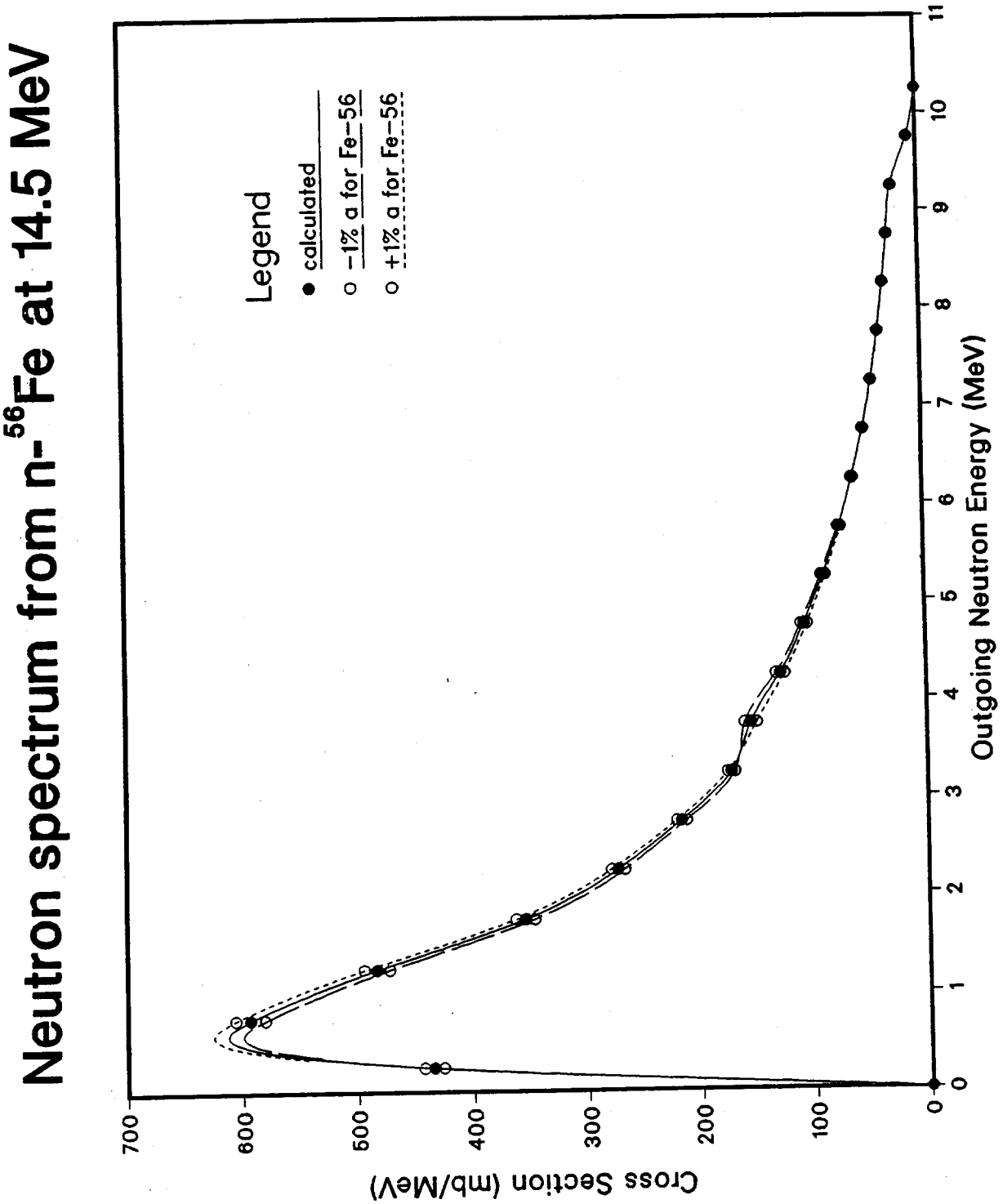

Fig. 39 Proton emission spectrum at 14.5 MeV
Uncertainty of ±1% was assumed for the a parameter for ^{56}Fe.

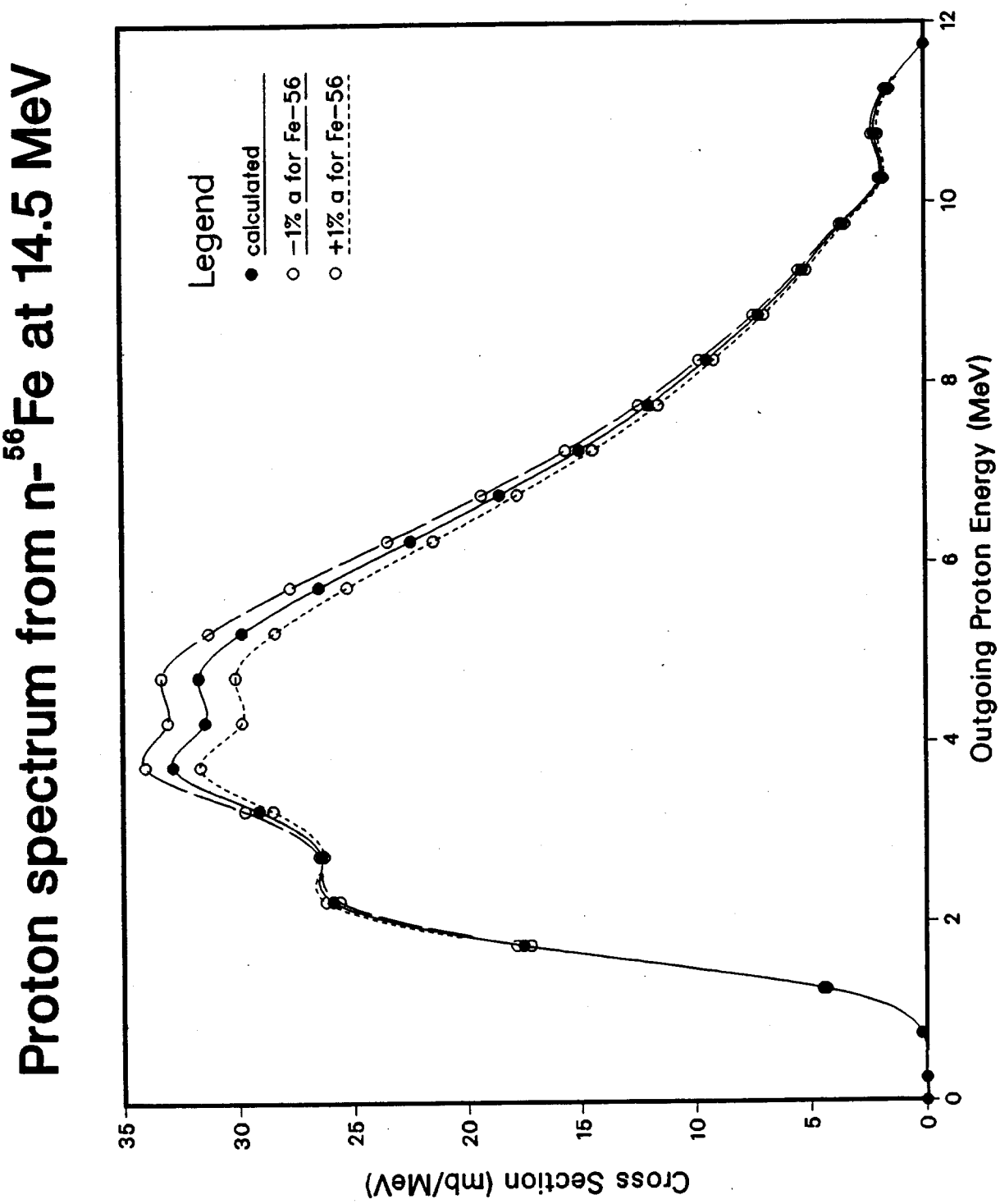

Fig. 40 α-particle emission spectrum at 14.5 MeV
Uncertainty of ±1% was assumed for the a parameter for ^{56}Fe.

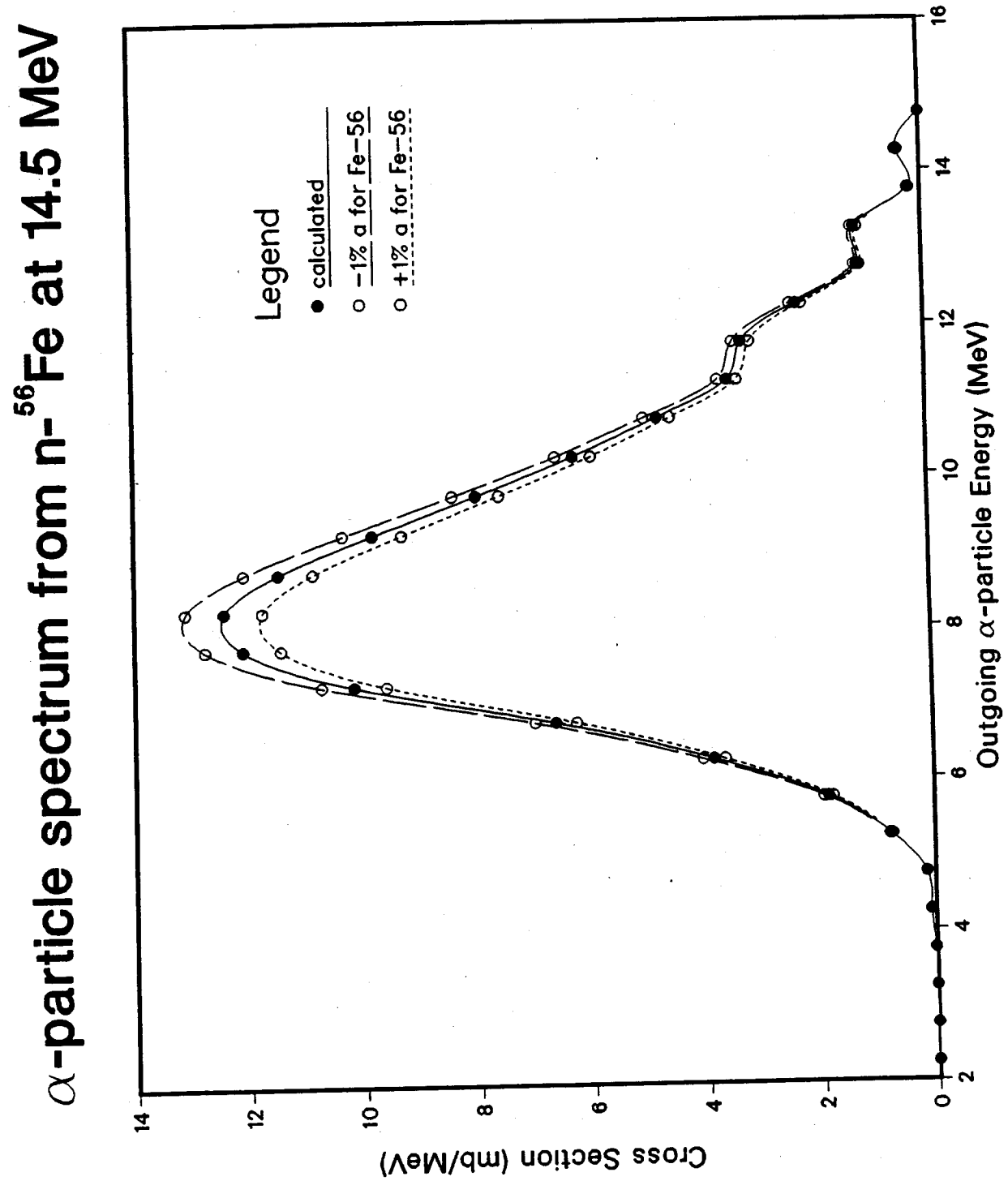

Fig. 41 γ-ray emission spectrum at 14.5 MeV
Uncertainty of ±1% was assumed for the a parameter for ^{56}Fe.